AGU PUBLICATIONS

Tectonics

RESEARCH ARTICLE
10.1002/2017TC004594

Sediment underthrusting within a continental magmatic arc: Coast Mountains batholith, British Columbia

David M. Pearson[1], Douglas R. MacLeod[1], Mihai N. Ducea[2,3], George E. Gehrels[2], and P. Jonathan Patchett[2]

[1]Department of Geosciences, Idaho State University, Pocatello, Idaho, USA, [2]Department of Geosciences, University of Arizona, Tucson, Arizona, USA, [3]Department of Geology and Geophysics, University of Bucharest, Bucharest, Romania

Key Points:
- Metasedimentary rocks forming the framework of a substantial proportion of the Coast Mountains batholith correlate to Stikinia
- Underthrusting to midcrustal levels occurred from the retroarc side during Cretaceous time
- Retroarc underthrusting is important for introducing supracrustal rocks to batholithic roots

Supporting Information:
- Supporting Information S1
- Table S1

Correspondence to:
D. M. Pearson,
pearson@isu.edu

Citation:
Pearson D. M., D. R. MacLeod, M. N. Ducea, G. E. Gehrels, and P. Jonathan Patchett (2017), Sediment underthrusting within a continental magmatic arc: Coast Mountains batholith, British Columbia, *Tectonics*, *36*, doi:10.1002/2017TC004594.

Received 31 MAR 2017
Accepted 14 AUG 2017
Accepted article online 18 AUG 2017

Abstract Though continental magmatic arcs are factories for new continental crust, a significant proportion of continental arc magmas are recycled from supracrustal material. To evaluate the relative contributions of retroarc underthrusting and trench side partial sediment subduction for introducing supracrustal rocks to the middle and lower crust of continental magmatic arcs, we present results from the deeply exposed country rocks of the Coast Mountains batholith of western British Columbia. Prior work demonstrates that these rocks underwent widespread partial melting that contributed to the Coast Mountains batholith. We utilize U-Pb zircon geochronology, Sm-Nd thermochronology, and field-based studies to document the protoliths and early burial history of amphibolite and granulite-facies metasedimentary rocks in the Central Gneiss Complex. U-Pb detrital zircon data from the structurally highest sample localities yielded ~190 Ma unimodal age peaks and suggest that retroarc rocks of the Stikine terrane constitute a substantial portion of the Central Gneiss Complex. These supracrustal rocks underwent thrust-related burial and metamorphism at >25 km depths prior to ~80 Ma. These rocks may also be underlain at the deepest exposed structural levels by Upper Cretaceous metasedimentary rocks, which may have been emplaced as a result of trench side underplating or intraarc burial. These results further our understanding of the mechanisms of material transport within the continental lithosphere along Cordilleran subduction margins.

1. Introduction

Continental magmatic arcs host the most voluminous intermediate magmatism on Earth and, as such, are potential factories for new continental crust. However, isotopic (ε_{Nd}, $^{87}Sr/^{86}Sr$, and $\delta^{18}O$) and trace element data from arc rocks suggest that in spite of major asthenospheric contributions to these melts, a substantial (~50%) proportion of continental arc magmas are recycled from supracrustal material [*Ducea and Barton*, 2007; *Otamendi et al*., 2009; *Behn et al*., 2011; *Chapman*, 2016]; this material is likely introduced to arc roots via trench side partial sediment subduction or retroarc underthrusting [*Ducea*, 2001]. Assessment of the relative contribution of these trench side or retroarc end-members to Cordilleran arcs is critical for evaluating growth of the continental crust and how crustal material is redistributed or recycled at ocean-continent subduction margins [e.g., *Clift and Vannucchi*, 2004; *DeCelles et al*., 2009; *Hacker et al*., 2011]. However, middle and lower continental arc crust is rarely exposed [*Ducea et al*., 2015a]. One exception is the Central Gneiss Complex of western British Columbia (Figure 1) [*Hutchison*, 1970; *Roddick*, 1970], which represents exhumed middle crust of the Jurassic to early Cenozoic Coast Mountains batholith [*Armstrong*, 1988]. Despite the widespread exposure of granulite- and amphibolite-facies batholithic framework rocks, including migmatites that contributed significantly to arc melts [*Kenah*, 1979; *Selverstone and Hollister*, 1980; *Hollister*, 1982; *Hollister and Andronicos*, 2000; *Woodsworth et al*., 1983a], the protolith of Central Gneiss Complex rocks is unknown.

This study utilizes spatially controlled U-Pb zircon geochronology, Sm-Nd garnet thermochronology, and field investigations to evaluate the protolith and early burial history of metasedimentary rocks from the deepest exposed structural levels of the Coast Mountains batholith (Figure 1). These results demonstrate that much of the exposed Central Gneiss Complex consists of retroarc rocks of the Stikine terrane that underwent westward underthrusting beneath the Coast Mountains batholith prior to ~80 Ma. These rocks may be underlain at the deepest structural levels by Upper Cretaceous metasedimentary rocks that originated in the Pacific-North American trench and were metamorphosed at high grade shortly after deposition.

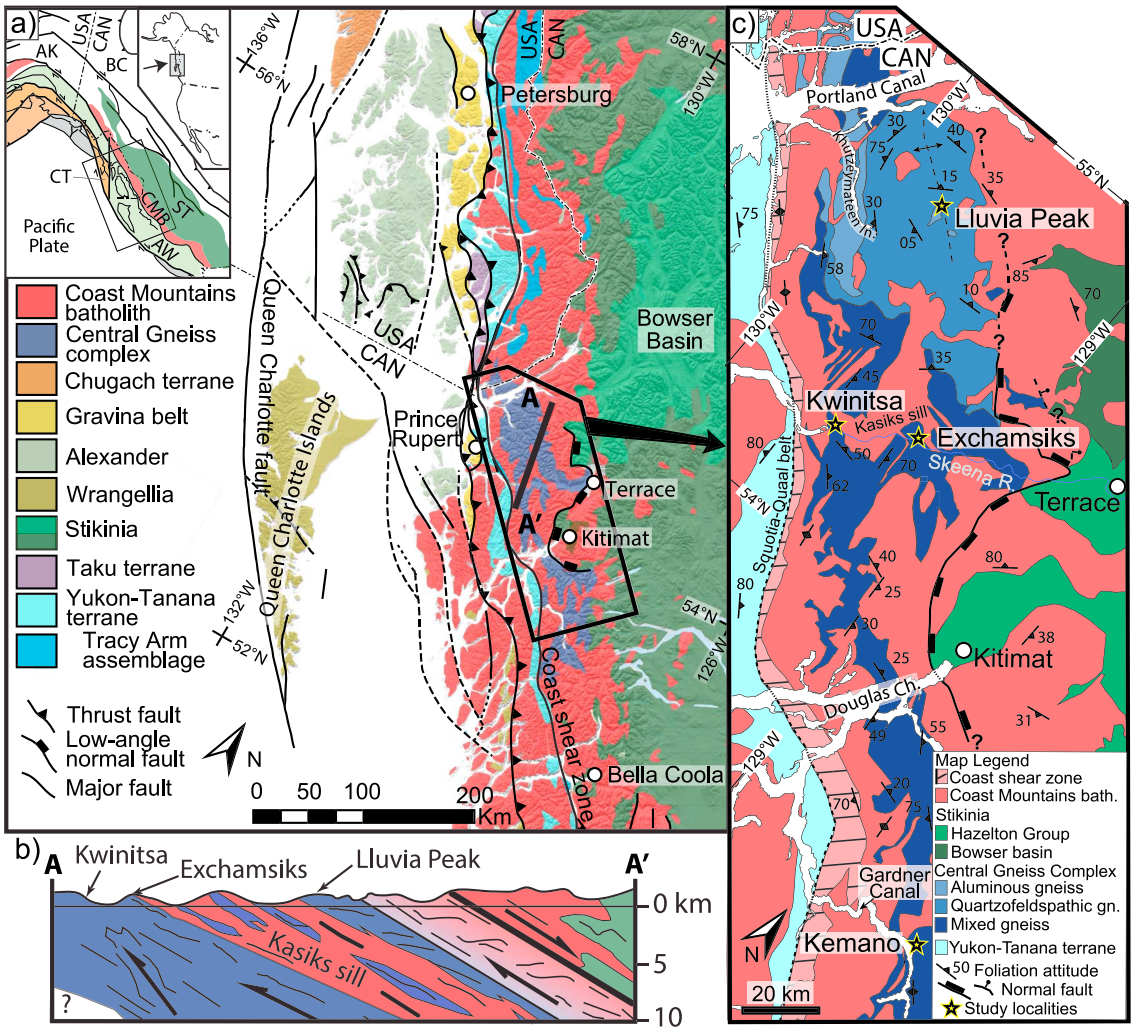

Figure 1. (a) Index map of the study area [after *Wheeler and McFeely*, 1991; *Gehrels et al*., 2009]. Inset abbreviations: AK, Alaska; AW, Alexander-Wrangellia terrane; BC, British Columbia; CMB, Coast Mountains batholith; CT, Chugach terrane; Y, Yakutat terrane. (b) A-A′ cross section showing relative structural positions of localities discussed in the text (modified from *Hollister and Andronicos* [1997]). (c) Geologic map of the Central Gneiss Complex (modified from *Roddick* [1970], *Hutchison* [1982], *Andronicos et al*. [2003], and *Rusmore et al*. [2005]). Skeena R., Skeena River; Douglas Ch., Douglas Channel; Khutzeymateen In., Khutzeymateen Inlet.

2. Geological Setting

The Coast Mountains batholith is a composite continental batholith intruded into the terrane-dominated margin of western British Columbia and southeastern Alaska [*Berg et al*., 1972; *Coney et al*., 1980; *Monger et al*., 1982; *Gehrels et al*., 2009]; the Central Gneiss Complex forms the high-grade metamorphic and igneous core of this batholith (Figure 1) [*Hutchison*, 1970, 1982; *Crawford and Hollister*, 1982; *Hollister*, 1982]. The Central Gneiss Complex is >230 km long, northwest-trending, and exposes midcrustal rocks as a result of major Eocene extension [*Heah*, 1991; *Andronicos et al*., 2003; *Rusmore et al*., 2005]. The Central Gneiss Complex is most studied in exposures along and south of the Skeena River [*Hutchison*, 1970, 1982; *Hollister*, 1975, 1977, 1982; *Hollister and Andronicos*, 1997, 2000; *Hollister and Burruss*, 1976; *Armstrong and Runkle*, 1979; *Kenah*, 1979; *Lappin and Hollister*, 1980; *Selverstone and Hollister*, 1980; *Woodsworth et al*., 1983a, 1983b; *Hill*, 1985a; *Crawford et al*., 1987; *Patchett et al*., 1998; *Andronicos et al*., 1999, 2003] but has also been studied along Douglas Channel [*Roddick*, 1970; *Rusmore et al*., 2005], Gardner Canal [*Depine et al*., 2011], and near Portland Canal [*Klepeis et al*., 1998]. Beyond earlier reconnaissance studies, several remote localities at higher elevations were also studied between the Skeena River and Portland Canal [*Hill*, 1985b; *Douglas*, 1986]. The northwestern and southeastern limits of the Central Gneiss Complex are poorly defined.

The Central Gneiss Complex is separated from rocks to the west by the Coast shear zone, which is a >1200 km long, steeply northeast-dipping structure with latest Cretaceous to Eocene reverse and likely strike-slip displacement and an earlier enigmatic deformation history [*Crawford and Hollister*, 1982; *Crawford et al*., 1987; *Gehrels et al*., 1991; *Klepeis et al*., 1998; *Rusmore et al*., 2001]. The eastern boundary of the Central Gneiss Complex, where studied, is a major Eocene extensional shear zone and detachment fault whose hanging wall is the Stikine terrane (Figure 1) [*Heah*, 1991; *Andronicos et al*., 2003; *Rusmore et al*., 2005].

2.1. Terrane Framework

The western margin of North America in the region of interest is an amalgamation of terranes. Terranes west of the Central Gneiss Complex near the latitude of Prince Rupert are confidently correlated to the Wrangellia, Alexander, Yukon-Tanana, and Taku terranes (Figure 1) [*Monger et al*., 1982, 1991; *Wheeler and McFeely*, 1991; *Gehrels*, 2001; *Gehrels and Saleeby*, 1987; *Gehrels et al*., 1990]. These western terranes largely consist of Neoproterozoic to middle Paleozoic arc-related rocks, Devonian to Permian carbonate and interbedded clastic sedimentary rocks, Triassic volcanic and sedimentary rocks, and unconformably overlying Upper Jurassic to Lower Cretaceous clastic strata and mafic volcanic rocks of the Gravina belt [e.g., *Gehrels*, 2001]. Clastic sedimentary rocks and younger rocks sourced from these terranes (e.g., Gravina belt) are characterized by abundant Neo- to Paleo-proterozoic and Devonian detrital zircon (DZ) grains [*Kapp and Gehrels*, 1998; *Gehrels*, 2000, 2002; *Gehrels et al*., 1990, 1991, 1992; *Tochilin et al*., 2014; *White et al*., 2015; *Yokelson et al*., 2015; *Giesler et al*., 2016; *Pecha et al*., 2016]. Northwest of these terranes and ~300 km northwest of the Central Gneiss Complex, translated slivers of >205–125 Ma metamorphic rocks and 101–55 Ma clastic sedimentary rocks constitute the Chugach terrane [*Berg et al*., 1972; *Amato et al*., 2013]. The Chugach terrane is an accretionary complex formed during east-dipping subduction, largely outboard of the Coast Mountains batholith; the formation of this accretionary complex was coeval with major Late Cretaceous to early Cenozoic dextral translation along the Cordilleran margin [*Pavlis and Sisson*, 1995; *Cowan*, 2003; *Roeske et al*., 2003; *Haeussler et al*., 2006; *Pavlis and Roeske*, 2007; *Amato and Pavlis*, 2010; *Amato et al*., 2013; *Gasser et al*., 2011; *Kochelek et al*., 2011; *Scharman and Pavlis*, 2012; *Garver and Davidson*, 2015].

East of the Central Gneiss Complex is the Stikine terrane. Pre-Mesozoic rocks forming basement to the Stikine terrane (Stikine Assemblage of *Monger et al*. [1991]) near Terrace (Figure 1) consist of a lower Mississippian to Pennsylvanian intermediate to felsic volcanic and plutonic complex [*Heah*, 1991; *Pignotta et al*., 2010] and an overlying unit of uppermost Pennsylvanian to middle Permian limestone [*Monger et al*., 1991; *Nelson*, 2009]. Some distinctive characteristics of Stikinian basement include (1) a lack of any pre-Devonian rocks, which is reflected in DZ populations that lack pre-Devonian zircons [*Greig and Gehrels*, 1995; *Logan et al*., 2000; *Evenchick et al*., 2007; *Pignotta et al*., 2010], and (2) predominantly volcanic/plutonic Devonian and Carboniferous rocks [*Monger et al*., 1991; *Logan et al*., 2000; *Nelson*, 2009], as opposed to generally older, primarily marginal quartzites and carbonates of Yukon-Tanana terrane equivalents to the north and west [*Gehrels et al*., 1990; *Gareau*, 1991; *Gareau and Woodsworth*, 2000].

East of Terrace (Figure 1), Stikinian basement is overlain by Early Jurassic lower Hazelton Group volcanic rocks [*Tipper and Richards*, 1976; *Monger*, 1977; *Monger et al*., 1982, 1991; *Evenchick*, 1991a; *Logan et al*., 2000; *Gagnon et al*., 2012]. The lower Hazelton Group consists primarily of 200–190 Ma (timescale of *Gradstein et al*. [2012]) felsic volcanic strata with lesser mafic lava flows and rare interbedded carbonate [*Tipper and Richards*, 1976; *Gagnon et al*., 2012]. These rocks are overlain by clastic sedimentary rocks that define the upper Hazelton Group [*Tipper and Richards*, 1976; *Gagnon et al*., 2012], which is, in turn, overlain by Upper Jurassic to latest Cretaceous clastic sedimentary rocks of the Bowser and Sustut basins [*Tipper and Richards*, 1976; *Monger*, 1977; *Monger et al*., 1982, 1991; *Evenchick*, 1991a; *Logan et al*., 2000].

Approximately 400 km northwest and along-strike of the Central Gneiss Complex, amphibolite-facies paragneiss, schist, and marble of the Tracy Arm terrane (*Berg et al*. [1978]; renamed as the "Tracy Arm assemblage" by *Gehrels et al*. [1991]) were correlated with the Yukon-Tanana terrane across the Coast shear zone on the basis of gradational contacts with stratigraphically overlying Permian and Triassic volcanic rocks and a distinctive abundance of Paleoproterozoic DZs [*McClelland et al*., 1992a; *Gehrels*, 2000, 2002; *Gehrels et al*., 1992; *Giesler et al*., 2016; *Pecha et al*., 2016]. However, an along-strike correlation of these rocks with the Central Gneiss Complex is complicated by the uncertain northwestward continuation of a major normal fault that bounds the northeastern margin of the Central Gneiss Complex (Figure 1). Though some authors [e.g., *Samson et al*., 1991] have proposed that the Yukon-Tanana terrane in southeastern Alaska represents

basement to the isotopically juvenile Stikine terrane, the lack of Devonian and Precambrian DZs in Stikinian rocks [*Evenchick et al*., 2007; *Barresi et al*., 2015; *Cutts et al*., 2015] makes this scenario unlikely.

2.2. Prior Constraints on Protolith of Central Gneiss Complex

In contrast to the confidently correlated terranes to the northeast and southwest, amphibolite- to granulite-facies rocks within the Central Gneiss Complex have evaded placement within a regional tectonostratigraphic framework due to high-grade metamorphism and Jurassic to Eocene magmatism. Adjacent terranes are difficult to trace into the Central Gneiss Complex because it is bounded on both sides by major shear zones (Figure 1) [*Hollister*, 1982; *Hollister and Andronicos*, 2006; *Crawford and Hollister*, 1982; *Heah*, 1991; *Andronicos et al*., 2003; *Rusmore et al*., 2005].

Much of the Central Gneiss Complex consists of heterogeneously layered gray-weathering quartzofeldspathic gneiss with lesser aluminous, rusty-weathering garnet-biotite, calc-silicate, and amphibolite gneiss (Figure 1c) [*Baer*, 1968; *Hutchison*, 1982; *Woodsworth et al*., 1983a; *Hollister and Andronicos*, 2000]. The aluminous gneiss has been extensively studied near the Skeena River [*Hollister and Andronicos*, 2000, and references therein] and is hypothesized to be a highly aluminous metasedimentary residuum left after partial melt extraction [*Selverstone and Hollister*, 1980; *Hollister and Andronicos*, 2000]. In addition to the presence of these aluminous metasedimentary rocks, carbonate is also interlayered with quartzofeldspathic gneiss, with one documented locality of preserved crinoid fossils [*Hill*, 1985a]. Near Lluvia Peak (Figure 1), *Hill* [1985b] also described a stretched-pebble conglomerate in quartzofeldspathic gneiss, which contains clasts that are compositionally distinct from the matrix. These and other field observations, as well as whole rock geochemistry, have led most workers to suggest that the protolith of the Central Gneiss Complex was a thick package of felsic to intermediate calc-alkaline volcanic rocks with interlayered sedimentary rocks [*Woodsworth et al*., 1983a; *Hill*, 1985b; *Douglas*, 1986; *Hollister and Andronicos*, 2000]. These rocks are interspersed with compositionally homogeneous bodies interpreted to be orthogneisses [e.g., *Hutchison*, 1967].

In contrast to relatively discontinuous aluminous rocks exposed adjacent to the Skeena River, a $>$6 km thick package of aluminous metasedimentary rocks is also exposed near Khutzeymateen Inlet [*Douglas*, 1983, 1986; *Hutchison*, 1967, 1982]; similar rocks are exposed near Lluvia Peak where they are interlayered with carbonates and amphibolites [*Hill*, 1985b] (Figure 1c). Though within its spatial boundaries, these rocks contrast with the primarily quartzofeldspathic gneiss exposed throughout much of the Central Gneiss Complex [*Hutchison*, 1982] and were thus hypothesized to overlie it. Additional work on these rocks by *Douglas* [1983, 1986] along Khutzeymateen Inlet suggested that these rocks were in thrust contact with the rocks below; in contrast, similar rocks near Lluvia Peak were interpreted by *Hill* [1985b] to unconformably overlie quartzofeldspathic gneiss of the Central Gneiss Complex. Workers documented amphibolite-facies metamorphism of these rocks, like the classically defined Central Gneiss Complex below, and recognized that they were both deformed together [*Douglas*, 1983, 1986; *Hill*, 1985b]. *Douglas* [1986] and *Wheeler and McFeely* [1991] favored a correlation of these "outlier" rocks with the Gravina belt, *McClelland et al*. [1992c] preferred a correlation with the Yukon-Tanana terrane, and *Hill* [1985b] suggested a correlation with Mesozoic rocks atop the Stikine terrane. In addition to the outstanding question of their age, the nature of the contact with underlying rocks is also unknown.

Crawford et al. [2000] suggested a correlation of the Central Gneiss Complex to the Yukon-Tanana terrane west of the Coast Shear zone based upon a similar mid-Cretaceous history of thrusting and metamorphism and hypothesized stratigraphic linkages. However, the Central Gneiss Complex only locally exhibits "evolved" isotopic signatures that would support a correlation with the Yukon-Tanana terrane or distal, North American craton-derived sedimentary rocks [*Patchett and Gehrels*, 1998]. Instead, much of the Central Gneiss Complex and Coast Mountains batholith is isotopically juvenile [*Armstrong and Runkle*, 1979; *Patchett et al*., 1998; *Cecil et al*., 2011; *Girardi et al*., 2012], which hinted at a correlation with the Stikine terrane to the east or Gravina belt to the northwest [*Douglas*, 1986; *Wheeler and McFeely*, 1991]. *Woodsworth* [1979] proposed a transitional eastern contact between the Stikine terrane and the Central Gneiss Complex, but the intervening region is characterized by a ~10 km wide zone of intense faulting and numerous dike swarms. Early attempts yielded ambiguous Rb-Sr and U-Pb zircon ages (36 ± 40 Ma Rb-Sr whole-rock isochron age: *Armstrong and Runkle* [1979]; 97–66 Ma and 75–65 Ma concordant isotope dilution-thermal ionization mass spectrometry (TIMS) U-Pb zircon ages: *Woodsworth et al*. [1983b]).

2.3. Prior Constraints on Burial Mechanism of Central Gneiss Complex

Rocks exposed within and adjacent to the Central Gneiss Complex were subjected to up to ~1000 km of Late Jurassic to mid-Cretaceous sinistral displacement along northwest-striking faults [*Avé Lallemant and Oldow*, 1988; *Plafker et al*., 1989; *Monger et al*., 1994; *Chardon*, 2003; *Chardon et al*., 1999; *Butler et al*., 2006; *Gehrels et al*., 2009; *Wolf et al*., 2010; *Angen et al*., 2014; *Tochilin et al*., 2014; *Yokelson et al*., 2015; *Giesler et al*., 2016; *Pecha et al*., 2016; *White et al*., 2015]. This was followed by development of a southwest-vergent, mid-Cretaceous thrust belt associated with underthrusting of the Alexander-Wrangellia composite terrane, which is now located southwest of the Coast shear zone [*Crawford et al*., 1987, 2000; *Crawford and Hollister*, 1982]. Structurally higher, amphibolite-facies rocks within this thrust belt are located directly west of the Coast shear zone and grade westward into structurally lower, greenschist-facies rocks of the Wrangellia terrane [*Crawford and Hollister*, 1982; *Crawford et al*., 1987; *Hutchison*, 1982; *Gehrels et al*., 1992; *McClelland et al*., 1992b; *Rubin and Saleeby*, 1992; *Rubin et al*., 1990; *Butler et al*., 2006]. Prograde garnet growth associated with crustal thickening in the thrust belt occurred from 108 to 102 Ma [*Wolf et al*., 2010], and thrusting was complete by ~90 Ma [*McClelland et al*., 1992b]; these western rocks had mostly cooled below ~500°C by ~75 Ma [*Butler et al*., 2006].

Rocks east of the Central Gneiss Complex in the Stikine terrane also experienced major Early Cretaceous to early Cenozoic shortening, which was accommodated by the northeast-vergent Skeena fold-thrust belt [*Evenchick*, 1991a, 1991b; *Evenchick et al*., 2007]. The Skeena fold-thrust belt is interpreted as a major upper crustal retroarc fold-thrust belt that accommodated $>$160 km of westward underthrusting of Stikinia into the deeper levels of the Coast Mountains batholith [*Evenchick*, 1991a, 1991b; *Evenchick et al*., 2007]. Thus, both retroarc and trench side underthrusting have been proposed to contribute to burial of Central Gneiss Complex rocks.

The earliest deformation recorded in the Central Gneiss Complex consists of pervasive folding, vertical flattening, and kyanite-grade metamorphism interpreted to result from thrusting and burial to 25–30 km depth [*Hollister*, 1982; *Hollister and Andronicos*, 2000; *Crawford et al*., 1987; *Andronicos et al*., 1999; *Stowell and Crawford*, 2000; *Rusmore et al*., 2005]. This deformation began prior to ~90 Ma and lasted until 77–70 Ma, as constrained by U-Pb zircon ages of syndeformational orthogneisses and monazite inclusions in garnet along Douglas Channel [*Rusmore et al*., 2005]. This shortening was followed by slow isothermal decompression as sillimanite replaced kyanite during formation of kilometer-scale, northeast-plunging folds and steeply northeast-dipping foliations; this episode of deformation was interpreted to represent continued contraction during partitioned dextral transpression from ~70 to 59 Ma [*Selverstone and Hollister*, 1980; *Klepeis et al*., 1998; *Hollister and Andronicos*, 1997, 2000, 2006; *Andronicos et al*., 1999, 2003; *Rusmore et al*., 2005]. After ~60 Ma, rapid exhumation of the Central Gneiss Complex was accommodated by major northeast-oriented extension, which was concurrent with granulite-facies metamorphism and high-volume magmatism at deeper structural levels that lasted until ~48 Ma [*Heah*, 1991; *Andronicos et al*., 2003; *Rusmore et al*., 2005; *Gehrels et al*., 2009].

3. Methods

3.1. Field Studies in the Lluvia Peak Area

Given that much of the early burial history of the structurally deepest rocks in the area is obscured by Cretaceous to Eocene magmatism and metamorphism, we focused our field investigations on high-elevation, structurally shallower rocks exposed at Lluvia Peak that were previously studied in reconnaissance fashion by *Hutchison* [1982] and as a part of an unpublished PhD dissertation by *Hill* [1985b]. These prior investigations strongly suggested sedimentary and calc-alkaline volcanic protoliths for rocks exposed there; thermobarometry indicates that they experienced amphibolite-facies metamorphism [*Hutchison*, 1982; *Hill*, 1985b], which is lower grade than structurally deeper rocks [e.g., *Hollister*, 1975]. In the context of our field investigations, we collected samples for U-Pb zircon (detrital and igneous) geochronology.

3.2. U-Pb Zircon Geochronology

To constrain protolith ages of Central Gneiss Complex and "outlier" rocks within its boundaries, we used U-Pb zircon geochronology. We then evaluated these results in the context of models for how supracrustal rocks are redistributed or recycled within deep crustal levels of Cordilleran magmatic arcs. We focused on localities

where previous work had documented sedimentary protoliths, including at Lluvia Peak and from representative lithologies of Central Gneiss Complex rocks along the northern side of the Skeena River and on the northeastern shore of Gardner Canal at Kemano Bay (Figure 1). During DZ sample collection and processing, care was taken to exclude any veins or dikes suspected to be of an igneous origin. We also analyzed igneous zircons to place a younger limit on the timing of deformation at Lluvia Peak, which is an important constraint on the timing and mechanism of burial of Central Gneiss Complex rocks.

Mineral separations for U-Pb zircon geochronology were accomplished using standard crushing techniques, followed by passage over a Wilfley shaking table, Frantz magnetic separator, and density separation using methylene iodide. We acquired cathodoluminescence (CL) images of all samples prior to analysis to locate laser spots on texturally distinct domains of zircon grains. U-Pb geochronology was performed at the University of Arizona's Laserchron Center using Laser Ablation-Multicollector-Inductively Coupled Plasma Mass Spectrometry (LA-MC-ICPMS). Spot sizes of 25–35 μm were used for zircon cores, whereas 12 or 25 μm spots were used for smaller rims or growth domains identified on CL images. Additional details of mineral separation and U-Pb analysis are given in Text S1 in the supporting information.

Amphibolite to granulite-facies metamorphism experienced by the Central Gneiss Complex (temperatures ~750 ± 50°C) [*Hollister*, 1975, 1977; *Selverstone and Hollister*, 1980] was insufficient to reset the U-Pb system in our rocks via volume diffusion (closure temperature of ~950°C for our smallest analyzed zircon grains, ~30 μm radius) [*Cherniak and Watson*, 2000]. Thus, we consider two more likely processes to potentially affect the U-Pb isotopic system in zircon during metamorphism: (1) partial or complete Pb loss through fluid interaction during metamorphism [e.g., *Geisler et al*., 2007] or (2) solid-state recrystallization [e.g., *Schaltegger et al*., 1999].

Partial and less commonly complete Pb loss through fluid interaction has been shown to disturb the U-Pb isotopic system in zircon via a diffusion-reaction process in radiation-damaged zircon and/or through dissolution-reprecipitation at zircon rims [e.g., *Pidgeon*, 1992; *Mezger and Krogstad*, 1997; *Geisler et al*., 2007]. In most rocks that experience Pb loss, some grains retain a memory of their parent isotope compositions, resulting in discordant analyses. In addition, given that Pb loss is enhanced in high-U, radiation-damaged zircon [*Mezger and Krogstad*, 1997], greater Pb loss and therefore younger U-Pb zircon ages should correlate with higher U content where Pb loss occurs during fluid interaction. In contrast, during coupled dissolution-reprecipitation of zircon, textural observations of zircons on CL images should show patchy reaction zones where the U-Pb isotopic system has been reequilibrated [*Pidgeon*, 1992; *Geisler et al*., 2007]. Some authors have also documented solid-state recrystallization of zircon during granulite-facies metamorphism [*Schaltegger et al*., 1999; *Hoskin and Black*, 2000]; during this process, compositional zoning of zircon grains on CL images becomes overprinted by dark, featureless zircon, providing an indicator that this process has occurred [*Corfu et al*., 2003; *Hoskin and Schaltegger*, 2003]. Thus, the approach taken here that utilizes U-Pb zircon geochronology in the context of high-resolution CL imaging is well suited to capture premetamorphic ages of zircon grains and the extent of possible Pb loss or recrystallization during high-grade metamorphism.

Zircons analyzed here display compositional zoning in CL images (Figure 2). Where possible, we analyzed zircon cores and rims. After analysis, we acquired high-resolution CL images at the grain-scale to observe laser pits in the context of compositional zoning. When determining maximum depositional ages for rocks interpreted to have sedimentary protoliths, we excluded rim and core analyses that sampled CL domains interpreted to be metamorphic in origin (Figure 2). We assigned maximum depositional ages to the youngest age cluster in a sample defined by three or more overlapping analyses [*Dickinson and Gehrels*, 2009].

3.3. Sm-Nd Garnet Thermochronology

To evaluate the timing and duration of metamorphism in the Kwinitsa samples, we used Sm-Nd garnet thermochronology. To place the Sm-Nd garnet thermochronological results in a geological context, we characterized garnet compositional zoning in sample GJP-92 using an electron microprobe. For Sm-Nd garnet thermochronology, the isotopic ratios of $^{143}Nd/^{144}Nd$ and the trace element concentrations of Sm and Nd were measured by TIMS on whole rock samples and garnet separates at the University of Arizona [*Ducea et al*., 2003]. Additional details of electron microprobe and Sm-Nd analytical methods are available in Text S1.

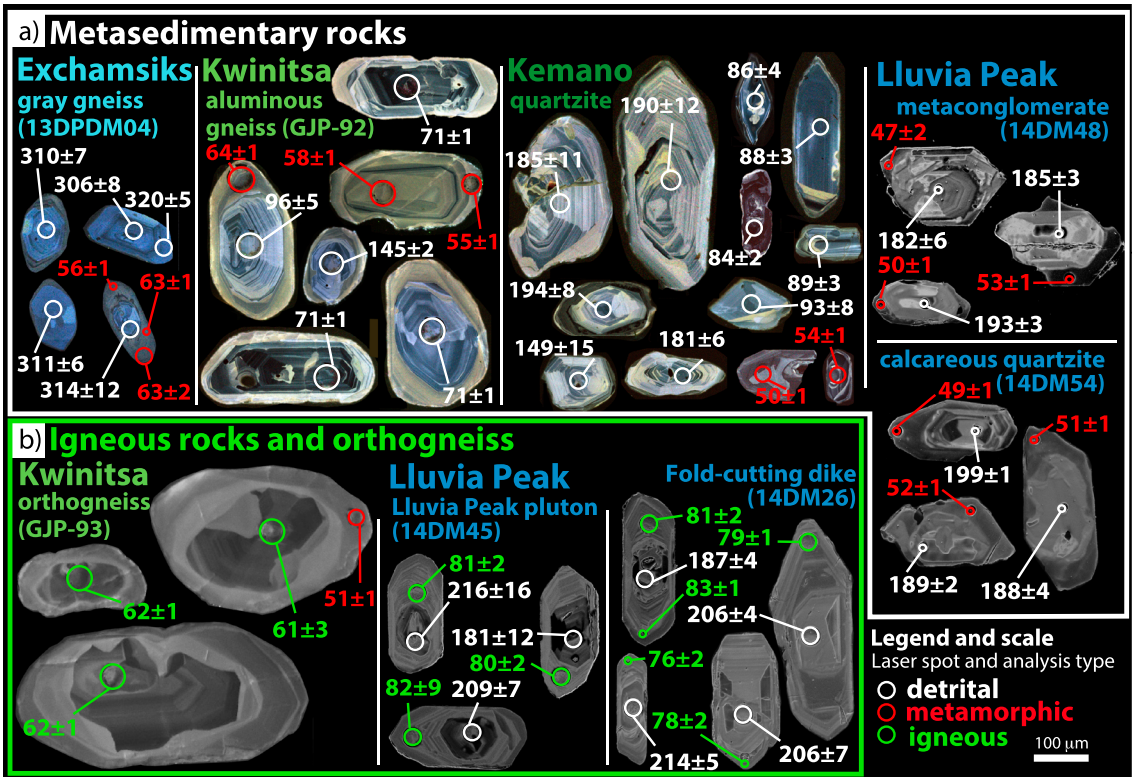

Figure 2. Representative cathodoluminescence images of zircons, with circles and dates denoting results from laser spots (analytical uncertainty at 1σ). CL images of zircons from (a) metasedimentary rocks and (b) igneous rocks and orthogneiss. Laser spot sizes: 35, 25, or 12 μm.

4. Results

Zircons in all samples analyzed here are generally elongate in shape; where present on CL images, zircon rim overgrowths overlap cores. Rim analyses generally yielded high U/Th ratios (≥10) and display minimal oscillatory zoning compared to zircon cores, an observation that is consistent with zircon crystallization during metamorphism [e.g., *Corfu et al*., 2003; *Rubatto*, 2002]. All gneissic samples analyzed here contain some zircons with pre- mid-Cretaceous core ages (Figures 2 and 3 and supporting information Table S1).

4.1. Lluvia Peak Area

4.1.1. Field Investigation

In the Lluvia Peak area, *Hutchison* [1967, 1982] and *Hill* [1985b] documented interlayered, "rusty-weathering" aluminous biotite schist and marble that overlies "gray-weathering" quartzofeldspathic gneiss characteristic of much of the Central Gneiss Complex elsewhere. In all of these lithologies, *Hill* [1985b] described shallowly west-plunging recumbent and isoclinal folds with wavelengths of centimeters to several hundred meters; gently west-dipping mylonitic foliations in the area are axial planar to these folds. Mineral and stretching lineations are also shallowly west-plunging and parallel the fold axes [*Hill*, 1985b]. *Hill* [1985b] also documented local migmatization and amphibolite-facies metamorphism (peak metamorphic conditions of 702 ± 50°C and 7.6 ± 1 kbar) using garnet-biotite thermometry and garnet-plagioclase-sillimanite-quartz barometry. Using detailed field and petrographic observations, *Hill* [1985b] interpreted the rocks in the area to preserve two phases of deformation: (1) earlier thrusting with uncertain kinematics across an approximately horizontal shear zone and (2) later, localized dextral transpression along northwest-striking structures. We conducted foot traverses above treeline along the northern side of the ridge connecting Epidote Crag, Lluvia Peak, and Niebla Peak and collected samples for geochronology and petrography. (Figure 4). This area constitutes a broad shear zone in the central portion of Hill's map area that she showed was largely unaffected by the second phase of deformation.

Several lines of evidence suggest that the largely quartzofeldspathic, structurally lower gneisses represent an interlayered sequence of felsic, metavolcanic, and metasedimentary rocks. For example, interlayered within

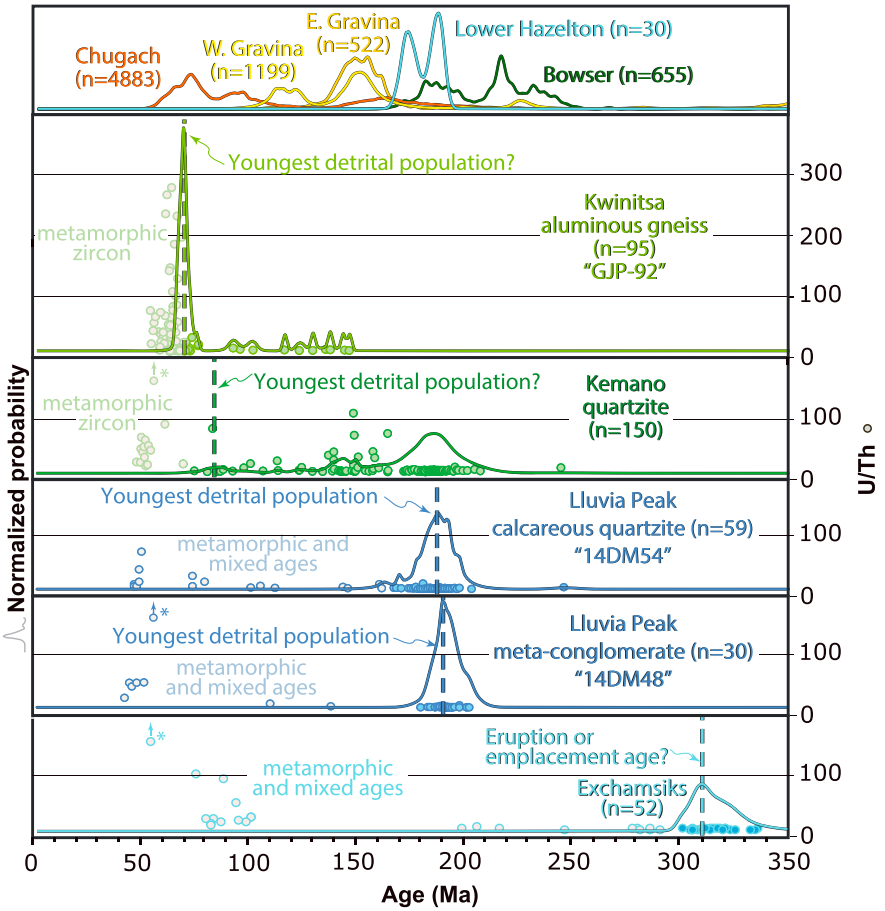

Figure 3. Normalized probability density plot and U/Th ratios for Central Gneiss Complex zircon analyses. Analyses interpreted to reflect metamorphic zircon growth were not included in probability plots and are shown in a lighter color. Data sources for reference strata: Gravina basin [*Kapp and Gehrels*, 1998; *Gehrels*, 2001; *Tochilin et al.*, 2014; *Yokelson et al.*, 2015], Bowser basin [*Evenchick et al.*, 2007], Chugach accretionary complex [*Haeussler et al.*, 2006; *Amato and Pavlis*, 2010; *Garver and Davidson*, 2015], and limited data from two detrital samples from the lower Hazelton Group with unimodal U-Pb zircon age populations [*Cutts et al.*, 2015].

the >1500 m thick dominant quartzofeldspathic lithology are 2–10 cm thick, boudinaged calcareous layers with epidote, diopside, and garnet rinds around crystalline calcite cores (Figure 5a) and aluminous layers with likely pelitic protoliths that contain abundant biotite, garnet, and sillimanite. In one locality (14DM03), 5–10 cm thick, repetitive layers of coarser grained, quartzofeldspathic gneiss transition into finer grained, more aluminous gneiss; this may be graded bedding (Figure 5b).

Structurally atop the quartzofeldspathic gneisses are >700 m of rusty-weathering aluminous gneisses previously interpreted to be metasedimentary rocks [*Hill*, 1985b; *Hutchison*, 1967, 1982]. These rocks consist of 0.3–4 m thick layers of fine-grained feldspathic quartzite, marble, calc-silicate gneiss, and uncommon medium-grained garnet-sillimanite-biotite gneiss (Figure 5c). Three continuous layers of amphibolite up to 30 m thick are also exposed (Figure 4). The rusty-weathering gneiss has an indistinguishable foliation from the quartzofeldspathic unit below and was subjected to the same peak metamorphic conditions [*Hill*, 1985b].

The most pervasive deformational fabrics exhibited by rocks in the area consist of shallowly west-dipping foliations that are parallel to the axial surfaces of isoclinal folds that deform compositional layering (Figure 4); the presence of rootless isoclinal folds (Figure 5d) attests to transposition of bedding. In addition to mineral and stretching lineations and fold axes, elongated clasts in a stretched pebble conglomerate (14DM48; Figure 5e) in the upper quartzofeldspathic gneiss are also shallowly west-plunging. In one location (14DM26), a 30 cm thick granodiorite dike crosscuts a meter-scale recumbent fold and exhibits a weak,

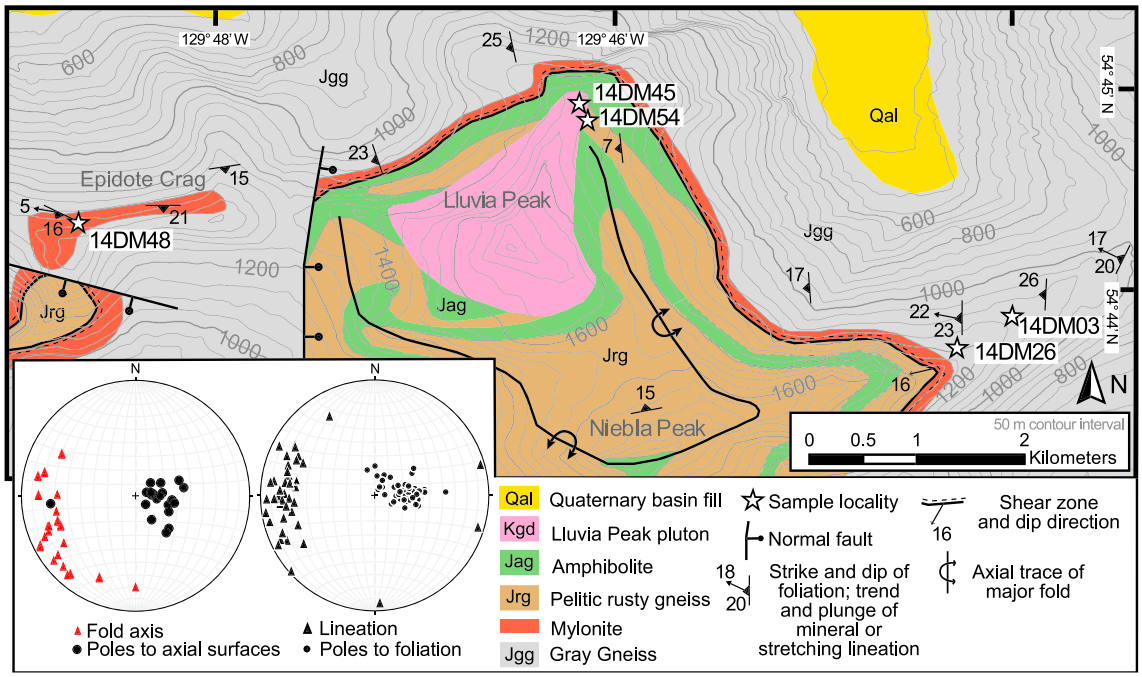

Figure 4. Geologic map of the Lluvia Peak area (modified from *Hill* [1985b]). Inset stereograms show lineations, fold axes, and poles to foliations and fold axial surfaces.

west-dipping foliation that parallels that in surrounding rocks (Figure 5f). These observations are in accord with *Hill* [1985b] and suggest that major strain occurred *before* granodioritic magmatism.

A prominent kilometer-scale, recumbent fold involving aluminous gneiss and amphibolite is obliquely truncated at the lithologic contact between the quartzofeldspathic and overlying aluminous gneiss, which is a zone of localized shear strain (Figure 4). Though the sill-shaped, granodioritic Lluvia Peak pluton cannot be directly observed to crosscut the mylonitized contact of the quartzofeldspathic and aluminous gneisses, the pluton is undeformed and clearly crosscuts the kilometer-scale fold. The intrusive contact of the pluton and adjacent gneisses is well-exposed (Figure 5g), and adjacent rocks are not contact-metamorphosed. Further, mylonites adjacent to the pluton have been statically recrystallized at the same regional metamorphic conditions as surrounding gneisses; these observations corroborate those of *Hill* [1985b] and indicate that the pluton postdates major folding and shear strain and that high-grade metamorphism of rocks in the area was synchronous with plutonism. Despite the importance of the age of the pluton for constraining the timing of deformation and metamorphism, prior age constraints are in conflict. Though *Hill* [1985b] reported a multigrain U-Pb zircon TIMS age of 77.1 ± 1.6 Ma ($^{206}Pb/^{238}U$, 2σ uncertainty), a more recent U-Pb zircon age obtained using LA-MC-ICPMS dating was 60 ± 13 Ma (Andronicos, 1997 unpublished data, reported in *Gehrels et al.* [2009]). The Lluvia Peak pluton also yielded a U-Pb titanite (closure temperature ≤ 750°C) [*Kohn and Corrie*, 2011; *Spencer et al.*, 2013] LA-MC-ICPMS age of 50.7 ± 1.5 Ma Andronicos,1997 unpublished data, reported in *Gehrels et al.* [2009]), and K-Ar hornblende and biotite ages of 53.7 ± 3.0 Ma and 51.9 ± 1.3 Ma, respectively [*Hill*, 1985b]. Given the inconsistency of the existing U-Pb zircon ages, we collected an additional sample (14DM45) for U-Pb zircon analysis to constrain the timing of deformation.

4.1.2. U-Pb Zircon Sample Context and Results

Samples collected from the Lluvia Peak area for U-Pb zircon geochronology consist of (1) quartzite from the previously described outcrop interpreted to exhibit graded bedding (DZ sample 14DM03); (2) calcareous quartzite from the rusty-weathering aluminous gneiss unit (DZ sample 14DM54); (3) stretched pebble conglomerate from the gray, quartzofeldspathic gneiss unit (DZ sample 14DM48); (4) a granodiorite dike cutting a recumbent fold, which puts a lower limit on the timing of isoclinal folding (14DM26); and (5) a sample of the undeformed Lluvia Peak pluton to place a younger limit on the timing of recumbent folding, major shear strain, and high-grade metamorphism.

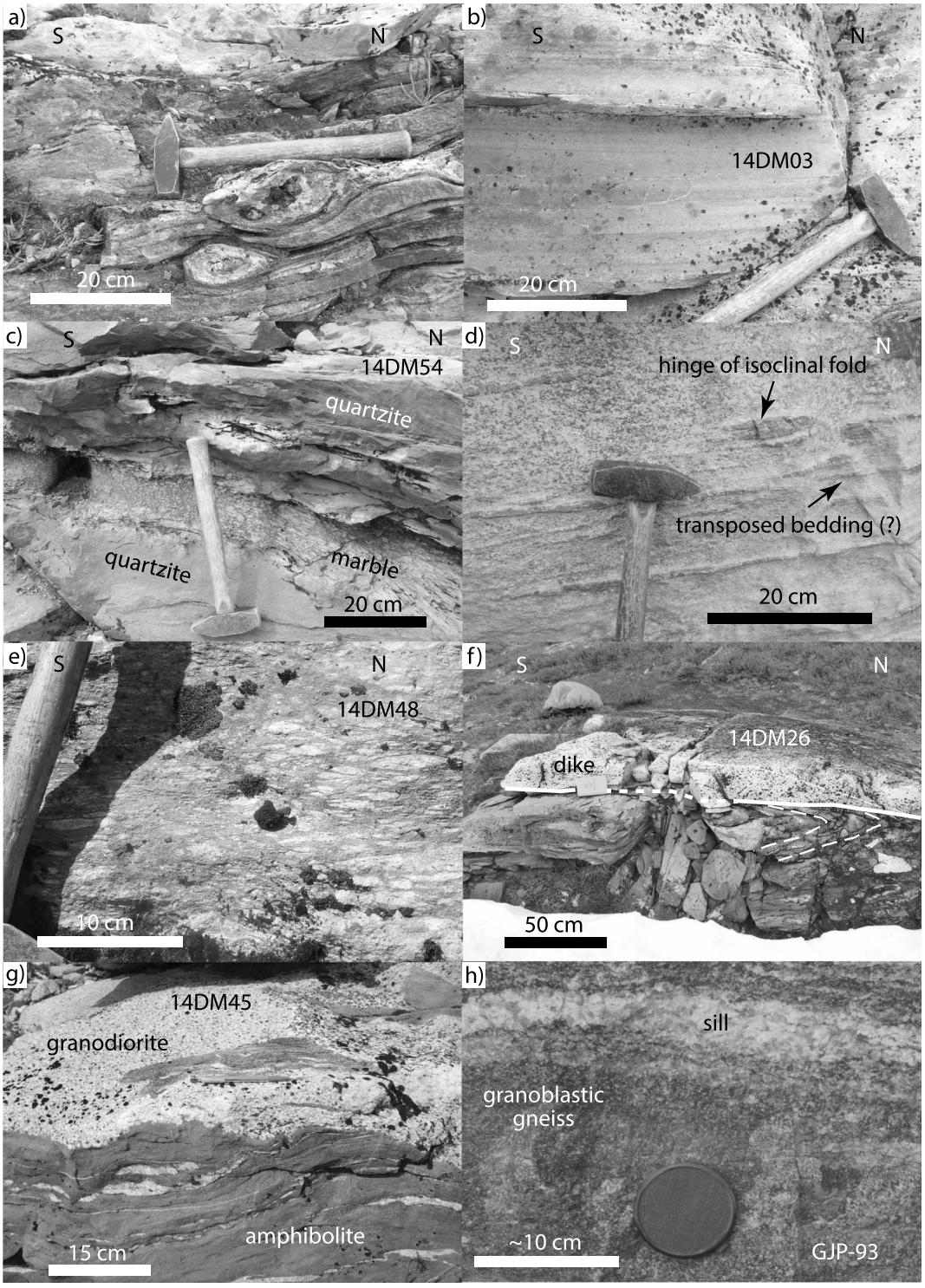

Figure 5. Field photos of Central Gneiss Complex rocks. Lluvia Peak: (a) boudinaged calcareous layers; (b) quartzite outcrop displaying apparent graded bedding (14DM03 sample locality); (c) outcrop of interlayered quartzite and marble (14DM54 sample locality); (d) rootless isoclinal folds and likely transposed bedding; (e) stretched pebble conglomerate (14DM48 sample locality); (f) granodiorite dike (14DM26 sample locality), which cuts an isoclinal fold; and (g) granodiorite of the Lluvia Peak pluton (14DM45 sample locality), which is undeformed and shown here at its intrusive contact with amphibolite of the upper metasedimentary sequence. Kwinitsa quarry: (h) granoblastic gneiss (GJP-93 sample locality).

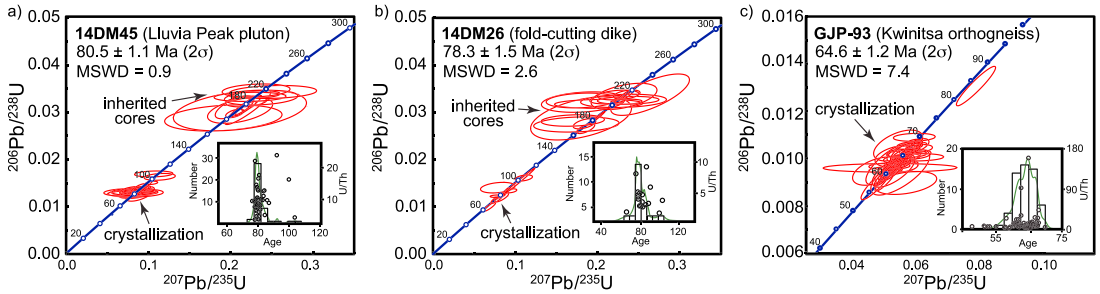

Figure 6. U-Pb concordia plots and mean U-Pb zircon ages of igneous rocks from Lluvia Peak area and orthogneiss from Kwinitsa quarry. Insets show U/Th ratios of analyses clustered near the interpreted crystallization age and probability density plots of analyses. (a and b) Lluvia Peak igneous rocks contain inherited zircon cores, with zircon rims interpreted to have grown during pluton crystallization. (c) The Kwinitsa orthogneiss is interpreted to have crystallized at ~65 Ma.

In general, zircon cores display oscillatory zoning, suggesting an original magmatic origin [*Corfu et al*., 2003]. The samples of stretched pebble conglomerate and calcareous quartzite both contain subhedral to rounded zircons with zoned cores surrounded by thick rims (Figure 2). We analyzed cores and rims in both samples; core analyses have low U/Th and rims have high U/Th (see supporting information Table S1). The sample of quartzite with apparent graded bedding did not yield many zircons, but four core analyses yielded an age of ~206 Ma (see supporting information Table S1). Core analyses from the stretched pebble conglomerate in the upper gray gneiss form a unimodal age peak at ~192 Ma (n = 30). Core analyses from the structurally highest metasedimentary DZ sample, the calcareous quartzite, yielded a prominent age peak at ~189 Ma (n = 59). Zircon rim analyses define an age of ~50 Ma. In sample 14DM54, an additional rim population may be present at ~80 Ma.

The granodiorite dike and the Lluvia Peak pluton both contain euhedral and elongate zircons (Figure 2), which either contain oscillatory zonation throughout or have inner, embayed cores mantled by oscillatory zoned rims. We dated cores and rims in both samples. In both samples, two age distributions are recognized: ~200 Ma igneous cores and ~80 Ma rims (Figure 6). Given the clear oscillatory zoned rims surrounding irregular, relict cores, we interpret the rim age to be representative of the age of crystallization. Interpreted as such, the pluton (14DM45) crystallization age is 80.5 ± 1.1 Ma (2σ error here and henceforth; n = 42) and the crosscutting dike is 78.3 ± 1.5 Ma (n = 11). The zircon ages are concordant for both samples and are statistically indistinguishable; our Lluvia Peak pluton crystallization age obtained here is similar to the 77.1 ± 1.6 Ma multigrain TIMS age reported by *Hill* [1985b].

4.2. Exchamsiks River U-Pb Zircon Sample Context and Results

We collected a sample (13DPDM04) from a medium-grained, garnet-biotite-hornblende-quartz-plagioclase gneiss ~1 km southwest of the Exchamsiks River that is structurally deeper in the Central Gneiss Complex compared to the Lluvia Peak locality [*Hollister and Andronicos*, 1997] and is located below the 53.4 ± 1.3 Ma Kasiks sill (Figure 1) [*Andronicos et al*., 2003]. The sample was described by *Woodsworth et al*. [1983a] as typical of gray-weathering quartzofeldspathic gneiss of the Central Gneiss Complex and was collected from a heterogeneously layered, well-foliated gneiss with ~10% mafic layers, up to 20 m thick carbonate layers, and occasional pegmatite sills. This locality is ~10 km southwest of the locality where *Hill*'s [1985a] crinoid fossil was collected. The Exchamsiks sample zircon cores are oscillatory zoned (Figure 2) and yielded a concordant, unimodal age population of 314 ± 5 Ma (n = 19); though rim dates vary from ~102 to ~56 Ma, apparently, two episodes of metamorphic zircon growth occurred at ~83 Ma and ~63–56 Ma (Figures 2 and 3).

4.3. Kwinitsa

4.3.1. U-Pb Zircon Sample Context and Results

Aluminous, dominantly metasedimentary lithologies from the deepest exposed crustal levels in the Central Gneiss Complex are well-exposed in the walls of a quarry at the Kwinitsa locality and, as such, have been extensively studied by prior workers [*Hollister*, 1975, 1977, 1982; *Armstrong and Runkle*, 1979; *Hutchison*, 1982; *Woodsworth et al*., 1983a, 1983b]. The outcrop here largely consists of layered biotite-garnet-plagioclase-quartz gneiss and lesser plagioclase-quartz-diopside orthogneiss [*Roddick and Hutchison*, 1972;

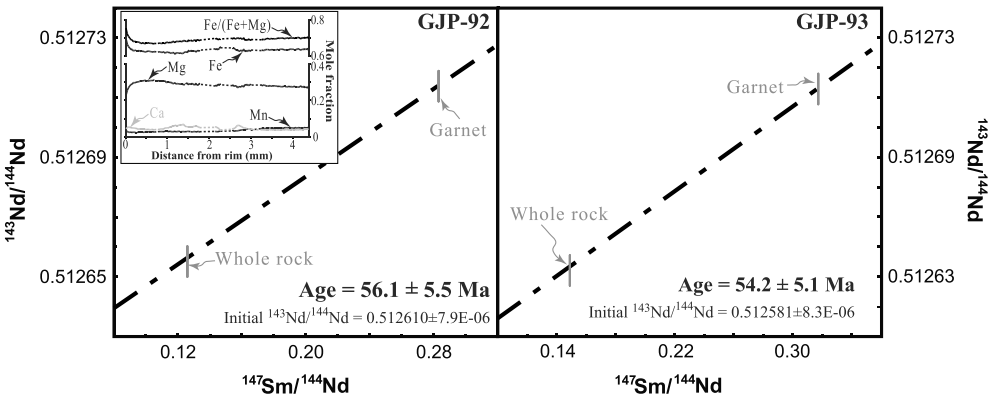

Figure 7. Garnet compositional zoning (inset) and garnet-whole rock isochron plots for aluminous paragneiss GJP-92 and orthogneiss GJP-93 from Kwinitsa area.

Hollister, 1975; *Woodsworth et al*., 1983a]. We collected two rocks from Kwinitsa quarry: sample GJP-92 was collected from a biotite-rich layer containing abundant purple garnet and fibrolitic sillimanite and graphite; this composition, in addition to the presence of interlayered, diopside-rich calcareous boudins, suggests a sedimentary protolith for these rocks [*Roddick and Hutchison*, 1972; *Woodsworth et al*., 1983a]. The second sample (GJP-93) was collected from a granoblastic gneiss consisting of plagioclase, quartz, diopside, biotite, and garnet (Figure 5h). This rock is very similar to orthogneiss described by others at the Kwinitsa locality, and we interpret it as such. Prior U-Pb multigrain TIMS ages of biotite-plagioclase-quartz gneiss and a pyroxene granulite from the quarry were reported by *Woodsworth et al*. [1983b]. Matrix zircons from those rocks yielded concordant ages of 65–58 Ma. In contrast, zircons from a garnet-bearing granulite that were primarily inclusions in garnet yielded ~75 Ma ages. Though these results were interpreted to reflect partial resetting of zircon included in garnet and full resetting of matrix zircon during metamorphism [*Woodsworth et al*., 1983b], the multigrain nature of the ages, internal zoning of the zircons observed on CL images, and lack of a textural context for these analyses prompted the work reported here.

Oscillatory zoned zircon cores in CL images of GJP-92 have low U/Th ratios and distinct, more homogeneous rims contain high U/Th (Figures 2 and 3 and supporting information Table S1). Core analyses yielded sparse U-Pb dates between 150 and 90 Ma, with a dominant age peak at ~71 Ma. Zircon rim analyses for this sample yielded high U/Th ratios and U-Pb dates that vary from ~69 Ma to ~55 Ma, with an average age of 64 ± 2 Ma (n = 10), which we interpret as the age of metamorphic zircon growth; this rock also contains an apparent ~56 Ma metamorphic zircon age population. The youngest population of core analyses contains low U/Th ratios and an age of 71 ± 2 Ma (n = 11). For orthogneiss sample GJP-93, zircon cores are oscillatory or sector-zoned and are surrounded by homogeneous to oscillatory zoned rims (Figure 2). Core analyses yielded an age of 64.6 ± 1.2 Ma (Figure 6). Rim analyses yielded an age of 52.6 ± 2.5 Ma (n = 6). Notably, in sample GJP-93, some core and rim analyses have high U/Th. Though roughly consistent with *Woodsworth et al*.'s [1983b] TIMS results, these new data demonstrate a complex Late Cretaceous and early Cenozoic history of magmatism and metamorphism.

4.3.2. Sm-Nd Garnet Thermochronology Sample Context and Results

Garnet grains in sample GJP-92 from Kwinitsa quarry are compositionally homogeneous except for minor retrograde diffusion-zoned rims (Figure 7), indicating equilibration with surrounding minerals at high temperatures. This suggests that our obtained garnet isochron ages represent cooling ages. We used *Ganguly and Tirone*'s [1999] model to calculate an average closure temperature for Kwinitsa garnets of ~730°C (see Text S1 for discussion of the Sm-Nd garnet closure temperature calculations). This is within-error of the peak metamorphic temperature recorded by rocks in this area (750°C ± 25°C) [*Selverstone and Hollister*, 1980]. The sample interpreted to have a metasedimentary origin yielded a garnet-whole rock Sm-Nd age of 56.1 ± 5.5 Ma, and the orthogneiss yielded an age of 54.2 ± 5.1 Ma (Figure 6).

4.4. Kemano Bay U-Pb Zircon Sample Context and Results

The Kemano sample was collected ~125 km southeast of Kwinitsa along Gardner Canal near the mouth of Kemano Bay (Figure 1). These rocks are also at structurally deep levels of the Central Gneiss Complex. In this

portion of the Central Gneiss Complex, country rocks of the Coast Mountains batholith consist of rusty fine-grained gneiss and schist, minor garnet-sillimanite-biotite schist, diopside- and epidote-rich marble, and garnet-staurolite-kyanite schist [*Roddick*, 1970; *Depine et al*., 2011]. The Kemano sample was collected from a nonmigmatitic outcrop of biotite-plagioclase-quartz schist that displays layering on the 30 cm scale, with thin metapelitic horizons. The layering is interpreted to reflect original graded bedding of the schist's sedimentary protolith. Zircons from this sample vary from rounded to elongate in shape; though most zircons contain oscillatory zoned cores with thin, homogeneous rims, some grains exhibit convolute or mosaic textures (Figure 2) [*Corfu et al*., 2003]. Several age populations are present in this sample: ~190 Ma, ~150 Ma, ~85 Ma, and ~53 Ma (Figure 3). The youngest age population that consists of core analyses with low U/Th is 85 ± 3 Ma (n = 8). Textures on CL images and high U/Th suggest metamorphic zircon growth at ~53 Ma.

5. Discussion

5.1. Constraints on Protolith, Burial Mechanism, and Cordilleran Tectonics

5.1.1. Lluvia Peak and Exchamsiks River

Quartzofeldspathic and aluminous gneisses in the Lluvia Peak area contain compositional layering, conglomerate, local carbonate interlayers, possible primary sedimentary structures, and highly aluminous layers. Detrital zircon U-Pb geochronology from these rocks defines unimodal age populations and maximum depositional ages of ~190 Ma for both quartzofeldspathic and aluminous gneissic units in the study area. These results suggest an interlayered sequence of volcanic and sedimentary rocks, at least partially in a marine depositional environment and adjacent to a felsic volcanic center, which is consistent with prior conclusions by *Hutchison* [1982] and *Hill* [1985b].

The absence of Precambrian zircons in all of our samples precludes correlation with rocks of the Yukon-Tanana or Taku terranes [*Kapp and Gehrels*, 1998; *Giesler et al*., 2016; *Pecha et al*., 2016] or Gravina belt [*Yokelson et al*., 2015]. Instead, ages for metasedimentary rocks reported here closely match the age of the lower Hazelton Group in western Stikinia [*Evenchick et al*., 2004; *Gagnon et al*., 2012], which also displays unimodal DZ spectra of the same age [*Barresi et al*., 2015; *Cutts et al*., 2015]. Likewise, the lithologic sequence exposed at Lluvia Peak is an excellent match to the lower Hazelton Group directly east of the Central Gneiss Complex [*Gagnon et al*., 2012; *Barresi et al*., 2015]. There, the lower Hazelton Group consists of 5–15 m thick intermediate to felsic lava flows with occasional interbedded marine sediments; these rocks are overlain by Early Jurassic interbedded carbonate and basalt flows [*Tipper and Richards*, 1976; *Marsden and Thorkelson*, 1992; *Gagnon et al*., 2012].

Despite the documentation by *Hill* [1985b] of distributed shear strain throughout the area, the close match in U-Pb zircon ages of rocks across the lithologic contact within the shear zone suggests that it either did not accommodate major slip or was bedding-parallel and thus accommodated only minor structural relief. These deformational fabrics are cut by a granodiorite pluton and associated sills that are largely undeformed. Taken together, these results suggest that the majority of deformation here occurred prior to ~80 Ma. Though the shear zone could alternatively be an extensional structure, low-angle normal faulting in the region is Eocene in age and the >80 Ma age of deformation is more simply interpreted as concurrent with regional thrusting.

Inherited, ~200 Ma zircon cores from a dike and the Lluvia Peak pluton are the same as or slightly older than ages of country rocks. The lack of a contact aureole around the pluton suggests that high-grade metamorphism was ongoing at ~80 Ma. Xenocrystic zircons that are similar in age to surrounding rocks (~200 Ma) suggest that partial melting of rocks likely deeper than the emplacement level during peak metamorphism contributed to ~80 Ma plutonism. Existing U-Pb titanite and K-Ar hornblende and biotite ages from the Lluvia Peak pluton of ~50 Ma [*Hill*, 1985b; *Gehrels et al*., 2009] match the age of high U/Th zircon rims in metasedimentary rocks interpreted here to be metamorphic and indicate that rocks either remained at high temperatures (up to 750°C) until after ~50 Ma or experienced another, separate pulse of late metamorphism.

A unimodal population of Early Pennsylvanian zircon core ages obtained from the Exchamsiks sample locality agrees with the likely age of *Hill*'s [1985a] crinoid stems collected from calc-silicate boudins ~10 km to the northeast. Although the heterogeneous nature of the rock dated here and interlayered carbonate boudins suggest that it was originally a volcanic rock, it is not possible to exclude a plutonic origin. The rock's

Pennsylvanian age is most simply interpreted as correlative to Stikinia, the basement of which comprises Mississippian to Pennsylvanian intermediate to felsic volcanic and plutonic rocks [*Heah*, 1991; *Logan et al*., 2000; *Pignotta et al*., 2010] that are overlain by Pennsylvanian to middle Permian limestone [*Monger et al*., 1991; *Nelson*, 2009]. The excellent correlation of structurally higher Lluvia Peak rocks with the lower Hazelton Group to the east, in addition to this structurally lower Pennsylvanian gneiss, strongly supports a correlation of a substantial portion of the Central Gneiss Complex with the western Stikine terrane.

Our primary results suggest that Central Gneiss Complex rocks, which are bounded on their western side by the >1200 km long Coast shear zone, correlate to Stikinia rather than the Yukon-Tanana terrane. This is in contrast to the presence of Yukon-Tanana terrane-equivalent rocks (Tracy Arm assemblage-Yukon-Tanana "south" of *Pecha et al*. [2016]) east of the Coast Shear Zone in southeastern Alaska (Figure 1) [*Gehrels*, 2000, 2002; *Gehrels et al*., 1991, 1992; *Giesler et al*., 2016; *Pecha et al*., 2016]. Similar rocks located west of the Coast shear zone (e.g., Scotia-Quaal belt) are also confidently correlated to the southern Yukon-Tanana terrane [*Gareau and Woodsworth*, 2000; *Gehrels*, 2001; *Giesler et al*., 2016; *Pecha et al*., 2016]. These rudimentary observations are consistent with apparent left-lateral separation of the two equivalent pieces of the southern Yukon-Tanana terrane across the Coast shear zone (Figure 1). This is consistent with prior stratigraphic and magmatic [*Avé Lallemant and Oldow*, 1988; *Plafker et al*., 1989; *Monger et al*., 1994; *Gehrels et al*., 2009; *Tochilin et al*., 2014; *White et al*., 2015; *Yokelson et al*., 2015; *Giesler et al*., 2016; *Pecha et al*., 2016] as well as structural observations [*Chardon*, 2003; *Chardon et al*., 1999; *Angen et al*., 2014] that demonstrate major Late Jurassic to Early Cretaceous sinistral deformation adjacent to and southwest of the Coast shear zone.

Concurrent with or following sinistral displacement, the first phase of penetrative deformation preserved in the Lluvia Peak area is similar in many ways to an "early," but poorly dated episode of shortening and burial metamorphism described elsewhere in the Central Gneiss Complex [*Hollister*, 1982; *Crawford et al*., 1987; *Andronicos et al*., 1999; *Hollister and Andronicos*, 2000; *Stowell and Crawford*, 2000; *Rusmore et al*., 2005]. In the context of prior work, our results show that a substantial portion of the Central Gneiss Complex was derived from the east and underwent major deformation prior to ~80 Ma. This supports hypothesized westward underthrusting at the roots of the Skeena fold-thrust belt, which accommodated >160 km of Cretaceous underthrusting of Stikinia beneath the Coast Mountains batholith [*Evenchick et al*., 2007]. Given the peak metamorphic pressure of ~7.6 kbar for rocks near Lluvia Peak [*Hill*, 1985b], this suggests that after ~190 Ma deposition, supracrustal rocks were buried to a depth of ~28 km.

Dextral transpression [*Hill*, 1985b] after ~77–70 Ma [*Andronicos et al*., 1999, 2003; *Rusmore et al*., 2005] overprinted this older deformation at deeper structural levels. The presence of 55–48 Ma metamorphic overgrowths in zircons from metasedimentary rocks matches the age of a major magmatic flare-up and associated metamorphism in the Coast Mountains batholith [*Gehrels et al*., 2009; *Girardi et al*., 2012], which was concomitant with major, extension-related exhumation in the Central Gneiss Complex [*Hollister et al*., 1982; *Heah*, 1991; *Andronicos et al*., 2003; *Rusmore et al*., 2005].

5.1.2. Kwinitsa and Kemano

In contrast to likely Stikinia-affinity rocks constrained by the structurally higher Exchamsiks sample, the Kwinitsa and Kemano gneisses yielded surprisingly young Late Cretaceous zircon dates that are inconsistent with known protoliths in the Stikine terrane (Figure 3). Despite the granulite-facies metamorphism of these rocks, they are unlikely to have been diffusionally reset [*Cherniak*, 2003; *Cherniak and Watson*, 2000]. Textures on CL images and high U/Th ratios (Figures 2 and 3) suggest that zircon rims in these rocks are metamorphic [*Rubatto*, 2002] and formed from ~64 to 53 Ma. Older rim ages from Kwinitsa paragneiss are similar to ~65 Ma igneous cores from the adjacent orthogneiss (sample GJP-93). Thus, metamorphic zircon growth in the adjacent sample GJP-92 was concurrent with intrusion of this orthogneiss and metamorphic zircon growth continued in both samples into early Eocene time. Furthermore, some high U/Th zircon core analyses in GJP-93 may suggest that melting and zircon neocrystallization occurred during high-grade metamorphism. Younger, ~56 Ma metamorphic zircon growth occurred during Eocene magmatism in the Central Gneiss Complex. These results are in accord with prior work suggesting latest Cretaceous to Eocene high-grade metamorphism at the deepest exposed levels of the Central Gneiss Complex [*Gehrels et al*., 2009].

In the Kemano sample, the oldest population of Jurassic zircons is similar to the ~190 Ma unimodal U-Pb zircon age peak obtained from metasedimentary rocks in the Lluvia Peak area. However, the sample also

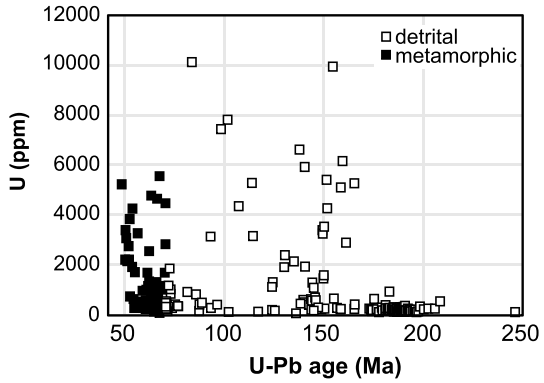

Figure 8. Uranium (ppm) versus U-Pb age for all analyses from paragneiss samples from Kemano Bay and Kwinitsa quarry (GJP-92). The lack of a correlation suggests that substantial Pb loss did not "reset" U-Pb zircon ages at the structurally deepest levels of the Central Gneiss Complex.

yielded many younger zircons. In paragneiss samples from Kemano and Kwinitsa (GJP-92), the lack of a correlation between U-content and U-Pb zircon core ages (Figure 8) and the observation that older and younger analyses are concordant (Figure S1 in the supporting information) suggest that Pb loss via fluid interaction did not produce the younger U-Pb zircon age populations. The populations of ~150 and 85 Ma Kemano zircons are characterized primarily by oscillatory zoning (Figure 2). However, some zircon cores also display convolute zoning and bleached CL domains that appear to overprint oscillatory zoned zircon cores. Kwinitsa paragneiss sample GJP-92 contains a dominant ~71 Ma population of grains that has oscillatory or planar-zoned cores and low U/Th ratios with an apparent lack of bleached domains; however, some zircons that yielded Early Cretaceous ages are also characterized by bleached portions of grains that overprint oscillatory zoned zircons. Elsewhere, others have observed similar bleached areas ("ghost textures") in CL images of zircon that seem to overprint oscillatory zoned zircon; the bleached areas are often located adjacent to dark, featureless domains on CL images where zircon may have undergone solid-state recrystallization [*Pidgeon*, 1992; *Schaltegger et al*., 1999; *Hoskin and Black*, 2000]. Interpreted in this context, this prior work interpreted the transitional bright domains adjacent to clearly defined older "protolith" zircon to represent high-grade metamorphic disturbance preceding incursion of solid-state recrystallization fronts toward grain interiors [*Schaltegger et al*., 1999; *Hoskin and Black*, 2000; *Geisler et al*., 2007].

To interpret the U-Pb zircon results from the Kwinitsa and Kemano paragneiss samples, we note that both samples contain oscillatory zoned zircon cores that predate well-defined metamorphic rims. In contrast to dark, featureless zircon documented elsewhere in high-grade metamorphic rocks that may have been modified during solid-state recrystallization [e.g., *Schaltegger et al*., 1999; *Hoskin and Black*, 2000], zircon imaged here apparently retained internal CL domains with oscillatory zoning. In addition, in the Kemano sample, U-Pb zircon core dates define distinct age populations rather than broad spreads of dates, with fewer grains displaying possible evidence for syn-metamorphic solid-state recrystallization. These observations support the interpretation that pre ~64 Ma zircon cores represent DZ grains whose ages have not been affected by solid-state recrystallization and therefore predate high-grade metamorphism.

The alternative hypothesis for rocks at the Kwinitsa and Kemano localities is that some of the "younger" zircon cores were subjected to postdepositional recrystallization or complete Pb loss. This could have resulted in formation of ghost and convolute zoning textures exhibited by Late Jurassic and Early Cretaceous zircon cores. In this scenario, U-Pb dates obtained from older DZ would represent inherited "protolith" zircon, whereas zircons that yielded Late Cretaceous dates could represent partially or fully recrystallized zircon during $\leq$70 Ma high-grade metamorphism.

If our simpler interpretation is correct that pre-64 Ma, Late Cretaceous zircon in paragneisses at Kwinitsa and Kemano represents a young detrital population, this suggests that some rocks at the deepest exposed levels of the Central Gneiss Complex represent Upper Cretaceous sedimentary rocks that were rapidly buried and metamorphosed in Late Cretaceous and early Cenozoic time. The two dominant age populations in the Kemano sample, ~190 Ma and ~150 Ma, would suggest sediment sources generally in the region of the Coast Mountains batholith. However, our samples lack abundant Triassic dates that dominate DZ populations from the Bowser/Sustut retroarc basin [*Evenchick et al*., 2007] and have maximum depositional ages younger than Upper Jurassic to Lower Cretaceous sediments of the Gravina belt [*McClelland et al*., 1992a; *Kapp and Gehrels*, 1998] (Figure 3). Upper Cretaceous rocks of the southern Chugach accretionary complex, currently northwest of the Central Gneiss Complex, were derived from the Coast Mountains batholith, contain major

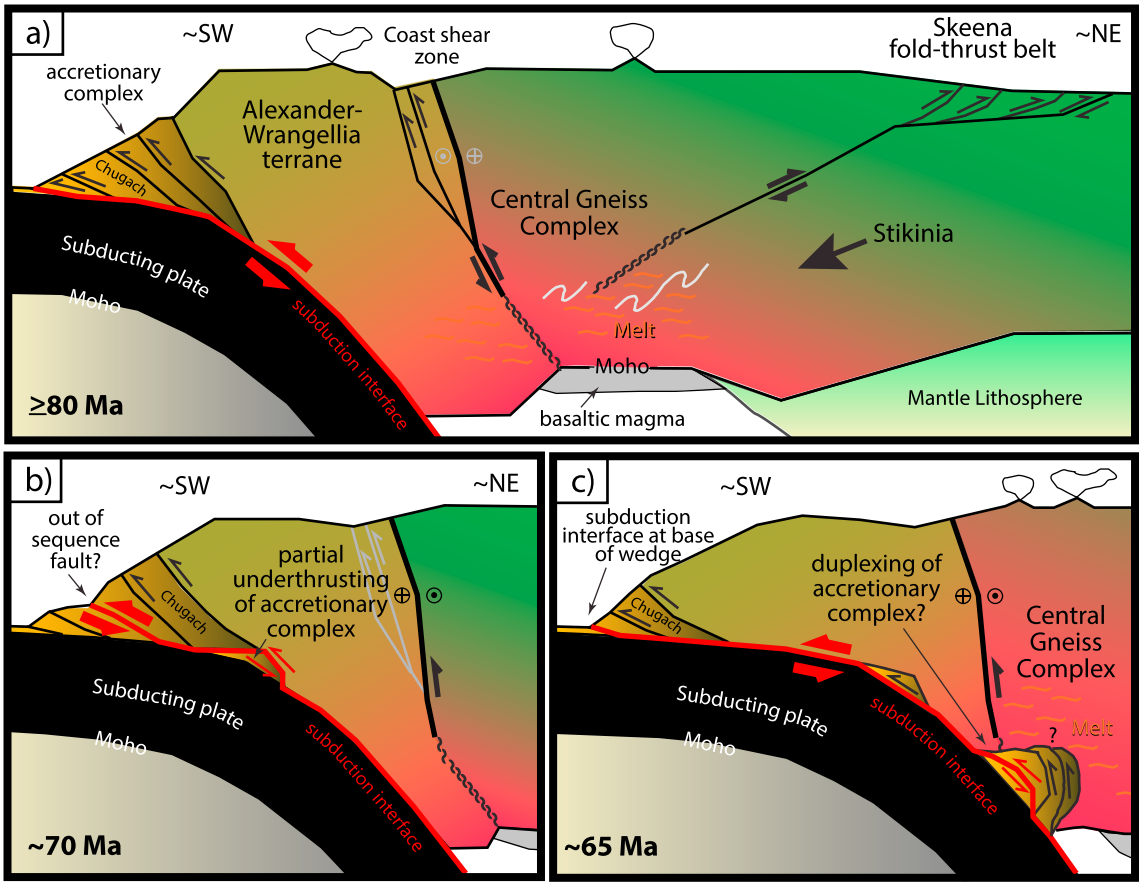

Figure 9. Tectonic cartoons showing: (a) retroarc underthrusting of Stikinia beneath the Coast Mountains batholith; (b and c) hypothesized underthrusting of forearc rocks, possibly correlative to the Chugach accretionary complex. Trench side underthrusting may have occurred during an episode of shallow subduction, activation of an out-of-sequence fault within the lower Chugach accretionary complex, and deep duplexing along the subduction interface.

age peaks that closely match our DZ populations, and are dominated in some samples by populations of Late Cretaceous ages very close to the depositional ages of the samples (Valdez Group) [*Haeussler et al.*, 2006; *Amato and Pavlis*, 2010; *Amato et al.*, 2013; *Kochelek et al.*, 2011; *Garver and Davidson*, 2015]. Thus, partial underthrusting of accretionary complex rocks [*Ducea et al.*, 2009], relamination of sediment at the plate interface [*Behn et al.*, 2011; *Hacker et al.*, 2011], or intraarc burial may also be a viable hypothesis for the burial of these rocks beneath the Coast Mountains batholith. Rocks with similar histories were also described from southern California [*Jacobson et al.*, 1996; *Barth et al.*, 2003; *Kidder and Ducea*, 2006], south-central Arizona [*Haxel et al.*, 2015], Idaho [*Lund et al.*, 2008], central Washington [*Matzel et al.*, 2004], southern Alaska [*Bleick et al.*, 2012; *Gasser et al.*, 2012], Argentina [*Cristofolini et al.*, 2012], and Tibet [*Kapp et al.*, 2003]. Structurally, the simplest interpretation for these metamorphic rocks is that they were underplated during shallow subduction (Figures 9b and 9c).

Prior work in the Kwinitsa area indicates that early regional metamorphism occurred at ≥10 kbar, followed by replacement of kyanite by sillimanite [*Hollister*, 1975, 1977, 1982]. In *Woodsworth et al.*'s [1983b] study of Kwinitsa rocks, zircon included in garnet yielded ~75 Ma ages, whereas matrix zircon was 65–58 Ma. Our results build upon this prior work and suggest that the younger matrix zircon grew during metamorphism that was contemporaneous with adjacent magmatism. Additional constraints on the Late Cretaceous metamorphic evolution of the Central Gneiss Complex come from the timing of garnet growth constrained by two samples at the Kwinitsa locality with garnet ages of ~55 Ma. Coupled with ages of metamorphic zircon, these results suggest that rocks did not cool below ~730°C until after ~55 Ma. Thus, these rocks were subjected to high-grade metamorphism on the order of 10 Ma, which was followed by rapid cooling during Eocene extension [*Heah*, 1991; *Andronicos et al.*, 2003; *Rusmore et al.*, 2005].

5.2. Lower Crustal Underplating of Accretionary Wedge Sediments

Though further work is needed to definitively exclude the possibility that zircons at the deepest exposed structural levels in the Central Gneiss Complex at Kemano and Kwinitsa underwent solid-state recrystallization (or complete Pb loss) during high-grade metamorphism, preliminary results suggest that Late Cretaceous trench side underthrusting may have occurred beneath the Coast Mountains batholith. Existing examples of trench side underplating emphasize an episode of shallow subduction [e.g., *Saleeby*, 2003]. The Late Cretaceous timing implied by these results predates early Cenozoic (~61–50 Ma) ridge subduction along the northern Cordilleran margin [e.g., *Bradley et al*., 1993; *Sisson and Pavlis*, 1993; *Haeussler et al*., 2003] and is broadly consistent with the timing of shallow subduction documented during the Laramide orogeny in the American southwest [e.g., *Yonkee and Weil*, 2015]. However, if these rocks were emplaced by a similar mechanism of shallow subduction, the implication is that (1) a northern corridor of shallow subduction, separate from that beneath the southwestern US, may have also occurred in Late Cretaceous time; (2) large parts of the Coast Mountains are regionally underlain by accretionary wedge material and that shallow subduction may have had a much wider North American footprint; or (3) an alternative emplacement mechanism, such as relamination [*Hacker et al*., 2011], is necessary.

5.3. Implications for Arc Magmatism

Results presented here suggest underthrusting of supracrustal rocks to $>$25 km depths, likely beneath the retroarc Skeena fold-thrust belt. The presence of abundant migmatites in Central Gneiss Complex rocks as well as elevated whole rock $\delta^{18}O$ isotopic data from the Coast Mountains batholith proper [*Wetmore and Ducea*, 2011] indicate that these or similar rocks contributed to the budget of arc magmatism. As such, these results support models of retroarc underthrusting for contributing upper plate material to Cordilleran arcs, perhaps aiding the development of flare-up events [*Ducea and Barton*, 2007; *DeCelles et al*., 2009; *Ducea et al*., 2015b].

Underthrusting of back arc or trench side sedimentary rocks and attachment to the lower crust of the upper plate of a subduction system has interesting consequences. Wet quartzofeldspathic sediments derived primarily from the volcanic arc are likely to undergo partial melting upon thermal relaxation in the lower crust on timescales on the order of ~10 Ma after burial [e.g., *Patiño Douce et al*., 1990]. Such metasedimentary materials begin melting at about 620°C [e.g., *Philpotts*, 1990], which is a temperature easily attainable in the middle and lower crust under orogenic areas [*Ducea et al*., 2015a]. Fundamentally, the replacement of an existing lower crust with one represented by metamorphosed first-cycle sediments can double the output of the magmatic arc. Melts produced in such scenarios have distinctive characteristics of S-type granitoids and if derived from the trench side will also have isotopic signatures indicative of interaction with seawater (elevated Sr and O isotopic ratios). In contrast to many ocean-continent orogenic systems [e.g., *Samson and Patchett*, 1991], country rocks of the Coast Mountains batholith are isotopically juvenile [*Armstrong and Runkle*, 1979; *Patchett et al*., 1998; *Cecil et al*., 2011; *Girardi et al*., 2012]. This resulted in a similarly juvenile character of the Coast Mountains batholith [e.g., *Girardi et al*., 2012]. In such a setting, these results emphasize the importance of radiometric tools like U-Pb dating of zircons to constrain the age and character of country rocks of Cordilleran batholiths.

6. Conclusions

Our results document that upper crustal materials from the continental (retroarc) side of the subduction system were transported to the deep levels of thickened continental crust under the Coast Mountains batholith. These materials may have provided a melt-fertile crustal component that enhanced the magmatic output of the arc. In addition, the deepest exposed rocks in the Central Gneiss Complex may have been underplated from the trench side during latest Cretaceous time. Together, these findings underscore the significance of transport of metasedimentary materials into the lower crust of the upper plate in subduction settings.

Acknowledgments
The data referenced in this paper are available in the text and supporting information. Additional information is available upon request to the corresponding author. This work was supported by NSF grant EAR-0309885 to M.D., G.G., and P.J.P.; Idaho State University to D.P.; Romanian National Science funding agency UEFISCDI grant PN-III-P4-ID-PCE-2016-0127 to M.D.; and NSF grant EAR-1338583 in support of the Arizona Laserchron Center. The Lluvia Peak portion of this work was conducted as part of an M.S. thesis by D.M. at Idaho State University. This manuscript benefitted from constructive comments from Lincoln Hollister, Bob Miller, an anonymous reviewer, associate editors Djordje Grujic and Sean Long, and editor John Geissman.

References

Amato, J. M., and T. L. Pavlis (2010), Detrital zircon ages from the Chugach terrane, southern Alaska, reveal multiple episodes of accretion and erosion in a subduction complex, *Geology*, *38*(5), 459–462, doi:10.1130/G30719.1.

Amato, J. M., T. L. Pavlis, P. D. Clift, E. J. Kochelek, J. P. Hecker, C. M. Worthman, and E. M. Day (2013), Architecture of the Chugach accretionary complex as revealed by detrital zircon ages and lithologic variations: Evidence for Mesozoic subduction erosion in south-central Alaska, *Geol. Soc. Am. Bull.*, *125*, 1891–1911, doi:10.1130/B30818.1.

Andronicos, C. L., L. S. Hollister, C. Davidson, and D. Chardon (1999), Kinematics and tectonic significance of transpressive structures within the Coast Plutonic Complex, British Columbia, *J. Struct. Geol.*, *21*(2), 229–243.
Andronicos, C. L., D. H. Chardon, L. S. Hollister, G. E. Gehrels, and G. J. Woodsworth (2003), Strain partitioning in an obliquely convergent orogen, plutonism, and synorogenic collapse: Coast Mountains batholith, British Columbia, Canada, *Tectonics*, *22*(2), 1012, doi:10.1029/2001TC001312.
Angen, J. J., C. R. van Staal, S. Lin, J. L. Nelson, J. B. Mahoney, D. W. Davis, and W. C. McClelland (2014), Kinematics and timing of shear zone deformation in the western Coast Belt: Evidence for mid-Cretaceous orogen-parallel extension, *J. Struct. Geol.*, *68*, 1–27, doi:10.1016/j.jsg.2014.05.026.
Armstrong, R. (1988), Mesozoic and early Cenozoic magmatic evolution of the Canadian Cordillera, in *Processes in Continental Lithospheric Deformation: A Symposium to Honor John Rodgers*, edited by S. P. Clark, B. C. Burchfiel, and J. Suppe, *Geol. Soc. Am. Bull. Spec. Pap.*, 218, 55–91.
Armstrong, R. L., and D. Runkle (1979), Rb-Sr geochronometry of the Ecstall, Kitkiata, and Quottoon plutons and their country rocks, Prince Rupert region, Coast Plutonic Complex, British-Columbia, *Can. J. Earth Sci.*, *16*(3), 387–399.
Avé Lallemant, H. G., and J. S. Oldow (1988), Early Mesozoic southward migration of Cordilleran transpressional terranes, *Tectonics*, *7*, 1057–1075.
Barth, A. P., J. L. Wooden, M. Grove, C. E. Jacobson, and J. N. Pedrick (2003), U-Pb zircon geochronology of rocks in the Salinas Valley region of California: A reevaluation of the crustal structure and origin of the Salinian block, *Geology*, *31*(6), 517–520.
Baer, A. (1968), Model of evolution of the Bella Coola-Ocean Falls region, Coast Mountains, British Columbia, *Can. J. Earth Sci.*, *5*, 1429–1441.
Barresi, T., J. L. Nelson, J. Dostal, R. Friedman, and H. Gibson (2015), Evolution of the Hazelton arc near terrace, British Columbia: Stratigraphic, geochronological, and geochemical constraints on a Late Triassic-Early Jurassic arc and Cu-Au porphyry belt, *Can. J. Earth Sci.*, *52*(7), 466–494, doi:10.1139/cjes-2014-0155.
Behn, M. D., P. B. Kelemen, G. Hirth, B. R. Hacker, and H.-J. Massonne (2011), Diapirs as the source of the sediment signature in arc lavas, *Nat. Geosci.*, *4*(9), 641–646, doi:10.1038/ngeo1214.
Berg, H. C., D. L. Jones, and D. H. Richter (1972), Gravina-Nutzotin Belt—Tectonic significance of an upper Mesozoic sedimentary and volcanic sequence in southeastern Alaska, *U.S. Geol. Surv. Prof. Pap., 800-D*, D1–D24.
Berg, H. C., D. L. Jones, and P. J. Coney (1978), Map showing pre-Cenozoic tectonostratigraphic terranes of southeastern Alaska and adjacent areas, *U.S. Geol. Surv. Open File Rep., 78-1085*, 1–20.
Bleick, H. A., A. B. Till, D. C. Bradley, P. O'Sullivan, J. L. Wooden, D. B. Bradley, T. A. Taylor, S. B. Friedman, and C. P. Hults (2012), Early Tertiary exhumation of the flank of a forearc basin, southwest Talkeetna Mountains, Alaska, *U.S. Geol. Surv. Open File Rep., 2012–1232*.
Bradley, D. C., P. J. Haeussler, and T. M. Kusky (1993), Timing of early Tertiary ridge subduction in southern Alaska, Geologic Studies in Alaska by the U.S. Geological Survey, in, *Geological Survey Bulletin*, vol. 2068, edited by C. Dusel-Bacon and A. B. Till, pp. 163–177, Washington, D. C.
Butler, R. F., G. E. Gehrels, W. Hart, C. Davidson, and M. L. Crawford (2006), Paleomagnetism of Late Jurassic to mid-Cretaceous plutons near Prince Rupert, British Columbia, in *Paleogeography of the North American Cordillera: Evidence for and Against Large-Scale Displacements*, edited by J. W. Haggart, R. J. Enkin, and J. W. H. Monger, *Geol. Assoc. Can. Spec. Pap.*, 46, 171–200, St. John's, NL, Canada.
Cecil, M. R., G. Gehrels, M. N. Ducea, and P. J. Patchett (2011), U-Pb-Hf characterization of the central Coast Mountains batholith: Implications for petrogenesis and crustal architecture, *Lithosphere*, *3*(4), 247–260, doi:10.1130/L134.1.
Chapman, A. D. (2016), The Pelona-Orocopia-Rand and related schists of southern California: A review of the best-known archive of shallow subduction on the planet, *Int. Geol. Rev.*, 1–38, doi:10.1080/00206814.2016.1230836.
Chardon, D. (2003), Strain partitioning and batholith emplacement at the root of a transpressive magmatic arc, *J. Struct. Geol.*, *25*(1), 91–107.
Chardon, D., C. L. Andronicos, and L. S. Hollister (1999), Large-scale transpressive shear zone patterns and displacements within magmatic arcs: The Coast Plutonic Complex, British Columbia, *Tectonics*, *18*(2), 278–292.
Cherniak, D. J. (2003), Diffusion in zircon, *Rev. Mineral. Geochem.*, *53*(1), 113–143, doi:10.2113/0530113.
Cherniak, D., and E. B. Watson (2000), Pb diffusion in zircon, *Chem. Geol.*, *172*, 5–24.
Clift, P., and P. Vannucchi (2004), Controls on tectonic accretion versus erosion in subduction zones: Implications for the origin and recycling of the continental crust, *Rev. Geophys.*, *42*, RG2001, doi:10.1029/2003RG000127.
Coney, P. J., D. L. Jones, and J. W. H. Monger (1980), Cordilleran suspect terranes, *Nature*, *288*(5789), 329–333, doi:10.1038/288329a0.
Corfu, F., J. Hanchar, P. Hoskin, and P. Kinny (2003), Atlas of zircon textures, *Rev. Mineral. Geochem.*, *53*, 469–500.
Cowan, D. (2003), Revisiting the Baranof-Leech River hypothesis for early Tertiary coastwise transport of the Chugach-Prince William terrane, *Earth Planet Sc Lett*, *213*, 463–475.
Crawford, M. L., and L. S. Hollister (1982), Contrast of metamorphic and structural histories across the Work Channel lineament, Coast Plutonic Complex, British-Columbia, *J. Geophys. Res.*, *87*, 3849–3860.
Crawford, M. L., L. S. Hollister, and G. J. Woodsworth (1987), Crustal deformation and regional metamorphism across a terrane boundary, Coast Plutonic Complex, British Columbia, *Tectonics*, *6*, 343–361.
Crawford, M. L., W. A. Crawford, and G. E. Gehrels (2000), Terrane assembly and structural relationships in the eastern Prince Rupert quadrangle, British Columbia, in *Tectonics of the Coast Mountains, Southeastern Alaska and British Columbia*, edited by H. H. Stowell and W. C. McClelland, *Geol. Soc. Ame. Spec. Pap.*, 1–21.
Cristofolini, E. A., J. E. Otamendi, M. N. Ducea, D. M. Pearson, A. M. Tibaldi, and I. Baliani (2012), Detrital zircon U-Pb ages of metasedimentary rocks from Sierra de Valle Fértil: Entrapment of Middle and Late Cambrian marine successions in the deep roots of the Early Ordovician Famatinian arc, *J. S. Am. Earth Sci.*, *37*(C), 77–94, doi:10.1016/j.jsames.2012.02.001.
Cutts, J. A., V. J. McNicoll, A. Zagorevski, and R. G. Anderson (2015), U-Pb geochronology of the Hazelton Group in the McTagg anticlinorium, Iskut River area, northwestern British Columbia, Geological Fieldwork, British Columbia Ministry of Energy and Mines, British Columbia Geological Survey Paper, 2015, 87–101.
DeCelles, P. G., M. N. Ducea, P. Kapp, and G. Zandt (2009), Cyclicity in Cordilleran orogenic systems, *Nat. Geosci.*, *2*(4), 251–257.
Depine, G. V., C. L. Andronicos, and L. S. Hollister (2011), Response of continental magmatic arcs to regional tectonic changes recorded by synorogenic plutons in the middle crust: An example from the Coast Mountains of British Columbia, *J. Struct. Geol.*, *33*(6), 1089–1104, doi:10.1016/j.jsg.2011.03.012.
Dickinson, W. R., and G. E. Gehrels (2009), Insights into North American paleogeography and paleotectonics from U-Pb ages of detrital zircons in Mesozoic strata of the Colorado Plateau, USA, *Int. J. Earth Sci.*, *99*(6), 1247–1265, doi:10.1007/s00531-009-0462-0.
Douglas, B. J. (1983), Structural and stratigraphic analysis of a metasedimentary inlier within the Coast Plutonic Complex, British Columbia, Canada, Princeton University Ph.D. thesis.
Douglas, B. J. (1986), Deformational history of an outlier of metasedimentary rocks, Coast Plutonic Complex, British Columbia, Canada, *Can. J. Earth Sci.*, *23*, 813–826.

Ducea, M. (2001), The California arc: Thick, granitic batholiths, eclogitic residues, lithospheric-scale thrusting, and magmatic flare-ups, *GSA Today*, *11*, 4–10.
Ducea, M. N., and M. D. Barton (2007), Igniting flare-up events in Cordilleran arcs, *Geology*, *35*(11), 1047–1050, doi:10.1130/G23898a.1.
Ducea, M. N., J. Ganguly, E. J. Rosenberg, P. J. Patchett, W. Cheng, and C. Isachsen (2003), Sm-Nd dating of spatially controlled domains of garnet single crystals: A new method of high-temperature thermochronology, *Earth Planet Sc. Lett.*, *213*(1–2), 31–42, doi:10.1016/S0012-821X(03)00298-X.
Ducea, M. N., S. Kidder, J. T. Chesley, and J. B. Saleeby (2009), Tectonic underplating of trench sediments beneath magmatic arcs: The central California example, *Int. Geol. Rev.*, *51*(1), 1–26, doi:10.1080/00206810802602767.
Ducea, M. N., S. R. Paterson, and P. G. DeCelles (2015a), High-volume magmatic events in subduction systems, *Elements*, *11*, 107–112, doi:10.2113/gselements.11.2.107.
Ducea, M. N., J. B. Saleeby, and G. Bergantz (2015b), The architecture, chemistry, and evolution of continental magmatic arcs, *Annu. Rev. Earth Planet. Sci.*, *43*(1), 150306093915001–33, doi:10.1146/annurev-earth-060614-105049.
Evenchick, C. A. (1991a), Structural relationships of the Skeena fold belt west of the Bowser Basin, northwest British Columbia, *Can. J. Earth Sci.*, *28*, 973–983.
Evenchick, C. A. (1991b), Geometry, evolution, and tectonic framework of the Skeena fold belt, north central British Columbia, *Tectonics*, *10*, 527–546.
Evenchick, C. A., M. A. McMechan, V. J. McNicoll, and S. D. Carr (2007), A synthesis of the Jurassic-Cretaceous tectonic evolution of the central and southeastern Canadian Cordillera: Exploring links across the orogen, in *Whence the mountains? Inquiries into the evolution of orogenic systems; a volume in honor of Raymond A. Price*, edited by J. W. Sears, T. A. Harms and C. A. Evenchick, *Geol. Soc. Am. Bull. Spec. Pap.*, 433, 117–145, doi:10.1130/2007.2433(06).
Evenchick, C. A., V. J. McNicoll, and L. D. Snyder (2004), Stratigraphy, geochronology, and geochemistry of the Georgie River area, northwest British Columbia, and implications for mineral exploration, *Can. J. Earth Sci.*, *41*(2), 199–216, doi:10.1139/e03-091.
Gagnon, J. F., T. Barresi, J. W. F. Waldron, J. L. Nelson, T. P. Poulton, F. Cordey, and M. Colpron (2012), Stratigraphy of the upper Hazelton Group and the Jurassic evolution of the Stikine terrane, British Columbia 11ESS contribution 20120051, *Can. J. Earth Sci.*, *49*(9), 1027–1052, doi:10.1139/e2012-042.
Ganguly, J., and M. Tirone (1999), Diffusion closure temperature and age of a mineral with arbitrary extent of diffusion: Theoretical formulation and applications, *Earth Planet. Sci. Lett.*, *170*(1–2), 131–140.
Ganguly, J., W. Cheng, and S. Chakraborty (1998), Cation diffusion in aluminosilicate garnets: Experimental determination in pyrope-almandine diffusion couples, *Contrib. Mineral. Petrol.*, *131*(2), 171–180, doi:10.1007/s004100050386.
Gareau, S. A. (1991), The Scotia-Quaal metamorphic belt: A distinct assemblage with pre-early Late Cretaceous deformational and metamorphic history, Coast Plutonic Complex, British Columbia, *Can. J. Earth Sci.*, *28*, 870–880.
Gareau, S. A., and G. J. Woodsworth (2000), Yukon-Tanana terrane in the Scotia-Quaal belt, Coast Plutonic Complex, central-western British Columbia, in *Tectonics of the Coast Mountains, southeastern Alaska and British Columbia*, edited by H. H. Stowell and W. C. McClelland, *Geol. Soc. Am. Bull. Spec. Pap.*, 343, 23–43, Denver, Colo.
Garver, J. I., and C. M. Davidson (2015), Southwestern Laurentian zircons in Upper Cretaceous flysch of the Chugach-Prince William terrane in Alaska, *Am. J. Sci.*, *315*(6), 537–556, doi:10.2475/06.2015.02.
Gasser, D., E. Bruand, K. Stüwe, D. A. Foster, R. Schuster, B. Fügenschuh, and T. Pavlis (2011), Formation of a metamorphic complex along an obliquely convergent margin: Structural and thermochronological evolution of the Chugach metamorphic complex, southern Alaska, *Tectonics*, *30*, TC2012, doi:10.1029/2010TC002776.
Gasser, D., D. Rubatto, E. Bruand, and K. Stüwe (2012), Large-scale, short-lived metamorphism, deformation, and magmatism in the Chugach metamorphic complex, southern Alaska: A SHRIMP U-Pb study of zircons, *Geol. Soc. Am. Bull. Bulletin.*, *124*(5–6), 886–905, doi:10.1130/B30507.1.
Gehrels, G. E. (2000), Reconnaissance geology and U-Pb geochronology of the western flank of the Coast Mountains between Juneau and Skagway, southeastern Alaska, in H. H. Stowell and W. C. McClelland, *Tectonics of the Coast Mountains, southeastern Alaska and British Columbia*, *Geol. Soc. Am. Bull. Spec. Pap.*, 343, 213–233.
Gehrels, G. E. (2001), Geology of the Chatham Sound region, southeast Alaska and coastal British Columbia, *Can. J. Earth Sci.*, *38*, 1579–1599.
Gehrels, G. E. (2002), Detrital zircon geochronology of the Taku terrane, southeast Alaska, *Can. J. Earth Sci.*, *39*(6), 921–931.
Gehrels, G. E., and J. B. Saleeby (1987), Geologic framework, tectonic evolution, and displacement history of the Alexander terrane, *Tectonics*, *6*, 151–173, doi:10.1029/TC006i002p00151.
Gehrels, G. E., W. C. McClelland, S. D. Samson, P. J. Patchett, and J. L. Jackson (1990), Ancient continental-margin assemblage in the northern Coast Mountains, Southeast Alaska and Northwest Canada, *Geology*, *18*(3), 208–211.
Gehrels, G. E., W. C. McClelland, S. D. Samson, and P. J. Patchett (1991), U-Pb geochronology of detrital zircons from a continental margin assemblage in the northern Coast Mountains, southeastern Alaska, *Can. J. Earth Sci.*, *28*(8), 1285–1300.
Gehrels, G. E., W. C. McClelland, S. D. Samson, P. J. Patchett, and M. J. Orchard (1992), Geology of the western flank of the Coast Mountains between Cape Fanshaw and Taku inlet, southeastern Alaska, *Tectonics*, *11*, 567–585, doi:10.1029/92TC00482.
Gehrels, G. E., V. A. Valencia, and J. Ruiz (2008), Enhanced precision, accuracy, efficiency, and spatial resolution of U-Pb ages by laser ablation-multicollector-inductively coupled plasma-mass spectrometry, *Geochem. Geophys. Geosyst.*, *9*, Q03017, doi:10.1029/2007GC001805.
Gehrels, G., et al. (2009), U-Th-Pb geochronology of the Coast Mountains batholith in north-coastal British Columbia: Constraints on age and tectonic evolution, *Geol. Soc. Am. Bull. Bulletin*, *121*(9–10), 1341–1361.
Geisler, T., U. Schaltegger, and F. Tomaschek (2007), Re-equilibration of zircon in aqueous fluids and melts, *Elements*, *3*(1), 43–50, doi:10.2113/gselements.3.1.43.
Giesler, D., G. Gehrels, M. Pecha, C. White, I. Yokelson, W. C. McClelland, and F. Corfu (2016), U-Pb and Hf isotopic analyses of detrital zircons from the Taku terrane, southeast Alaska, *Can. J. Earth Sci.*, *53*(10), 979–992, doi:10.1139/cjes-2015-0240.
Girardi, J. D., P. J. Patchett, M. N. Ducea, G. E. Gehrels, M. R. Cecil, M. E. Rusmore, G. J. Woodsworth, D. M. Pearson, C. Manthei, and P. Wetmore (2012), Elemental and isotopic evidence for granitoid genesis from deep-seated sources in the Coast Mountains batholith, British Columbia, *J. Petrol.*, *53*, 1505–1536, doi:10.1093/petrology/egs024.
Gradstein, F. M., J. G. Ogg, M. D. Schmitz, and G. M. Ogg (2012), *The Geologic Time Scale 2012*, Elsevier, Oxford, U. K.
Greig, C. J., and G. E. Gehrels (1995), U-Pb zircon geochronology of Lower Jurassic and Paleozoic Stikinian strata and Tertiary intrusions, northwestern British Columbia, *Can. J. Earth Sci.*, *32*(8), 1155–1171.
Hacker, B. R., P. B. Kelemen, and M. D. Behn (2011), Differentiation of the continental crust by relamination, *Earth Planet. Sci. Lett.*, *307*(3–4), 501–516, doi:10.1016/j.epsl.2011.05.024.

Haeussler, P., D. Bradley, R. Wells, and M. Miller (2003), Life and death of the resurrection plate: Evidence for its existence and subduction in the northeastern Pacific in Paleocene–Eocene time, *Geol. Soc. Am. Bull. Bulletin*, *115*(7), 867–880.

Haeussler, P. J., G. E. Gehrels, and S. M. Karl (2006), Constraints on the age and provenance of the Chugach accretionary complex from detrital zircons in the Sitka graywacke near Sitka, Alaska, in Studies by the U.S. Geological Survey in Alaska, 2004, *U.S. Geol. Surv. Prof. Pap.*, 1709-F.

Haxel, G. B. (2015), Mantle peridotite in newly discovered far-inland subduction complex, southwest Arizona: Initial report, *Int. Geol. Rev.*, *57*(5–8), 1–22, doi:10.1080/00206814.2014.928916.

Heah, T. S. T. (1991), Mesozoic ductile shear and Paleogene extension along the eastern margin of the Central Gneiss Complex, Coast Belt, Shames River Area, near Terrace, British Columbia, The University of British Columbia M.S. thesis.

Hill, M. L. (1985a), Remarkable fossil locality: Crinoid stems from migmatite of the Coast Plutonic Complex, British Columbia, *Geology*, *13*(11), 825–826.

Hill, M. L. (1985b), Geology of the Redcap Mountain area, Coast Plutonic Complex, British Columbia, Princeton University Ph.D. thesis.

Hollister, L. S. (1975), Granulite facies metamorphism in Coast Range Crystalline Belt, *Can. J. Earth Sci.*, *12*(11), 1953–1955.

Hollister, L. S. (1977), The reaction forming cordierite from garnet, the Khtada Lake metamorphic complex, British Columbia, *Can. Mineral.*, *15*, 217–229.

Hollister, L. S. (1982), Metamorphic evidence for rapid (2 mm/yr) uplift of a portion of the Central Gneiss Complex, Coast Mountains, BC, *Can. Mineral.*, *20*, 319–332.

Hollister, L. S., and C. Andronicos (2000), The Central Gneiss Complex, Coast Mountains, British Columbia, in *Tectonics of the Coast Mountains, southeastern Alaska and British Columbia*, edited by H. H. Stowell and W. C. McClelland, *Geol. Soc. Am. Bull. Spec. Pap.*, 343, 45–59.

Hollister, L. S., and C. L. Andronicos (1997), A candidate for the Baja British Columbia fault system in the Coast Plutonic Complex, *GSA Today*, *7*, 1–7.

Hollister, L. S., and C. L. Andronicos (2006), Formation of new continental crust in western British Columbia during transpression and transtension, *Earth Planet. Sci. Lett.*, *249*(1–2), 29–38.

Hollister, L. S., and R. C. Burruss (1976), Phase equilibria in fluid inclusions from the Khtada Lake metamorphic complex, *Geochim. Cosmochim. Acta*, *40*, 163–175.

Hoskin, P., and L. Black (2000), Metamorphic zircon formation by solid-state recrystallization of protolith igneous zircon, *J. Metamorph. Geol.*, *18*(4), 423–439.

Hoskin, P., and U. Schaltegger (2003), The composition of zircon and igneous and metamorphic petrogenesis, *Rev. Mineral. Geochem.*, *53*, 27–62.

Hutchison, W. W. (1967), Prince Rupert and Skeena map-areas, British Columbia, *Geol. Surv. Can. Pap.*, *66-33*, 1–27.

Hutchison, W. W. (1970), Metamorphic framework and plutonic styles in Prince Rupert region of the central Coast Mountains, British Columbia, *Can. J. Earth Sci.*, *7*(2), 376–405.

Hutchison, W. W. (1982), Geology of the Prince Rupert-Skeena map area, British Columbia, *Geol. Surv. Can. Mem.*, *394*, 116.

Jacobson, C. E., F. R. Oyarzabal, and G. B. Haxel (1996), Subduction and exhumation of the Pelona-Orocopia-Rand schists, southern California, *Geology*, *24*(6), 547–550.

Kapp, P. A., and G. E. Gehrels (1998), Detrital zircon constraints on the tectonic evolution of the Gravina belt, southeastern Alaska, *Can. J. Earth Sci.*, *35*, 253–268.

Kapp, P., A. Yin, C. E. Manning, T. M. Harrison, M. H. Taylor, and L. Ding (2003), Tectonic evolution of the early Mesozoic blueschist-bearing Qiangtang metamorphic belt, central Tibet, *Tectonics*, *22*(4), 1043, doi:10.1029/2002TC001383.

Kidder, S., and M. N. Ducea (2006), High temperatures and inverted metamorphism in the schist of Sierra de Salinas, California, *Earth Planet. Sci. Lett.*, *241*(3–4), 422–437, doi:10.1016/J.Epsl.2005.11.037.

Kenah, C. (1979), Mechanism and physical conditions of emplacement of the Quottoon pluton, British Columbia, Princeton Univ. PhD.thesis.

Klepeis, K. A., M. L. Crawford, and G. Gehrels (1998), Structural history of the crustal-scale coast shear zone north of Portland Canal, southeast Alaska and British Columbia, *J. Struct. Geol.*, *20*(7), 883–904.

Kochelek, E. J., J. M. Amato, T. L. Pavlis, and P. D. Clift (2011), Flysch deposition and preservation of coherent bedding in an accretionary complex: Detrital zircon ages from the Upper Cretaceous Valdez Group, Chugach terrane, Alaska, *Lithosphere*, *3*(4), 265–274, doi:10.1130/L131.1.

Kohn, M. J., and S. L. Corrie (2011), Preserved Zr-temperatures and U-Pb ages in high-grade metamorphic titanite: Evidence for a static hot channel in the Himalayan orogen, *Earth Planet Sc Lett*, *311*(1–2), 136–143, doi:10.1016/j.epsl.2011.09.008.

Lappin, A. R., and L. S. Hollister (1980), Partial melting in the Central Gneiss Complex near Prince Rupert, British Columbia, *Am. J. Sci.*, *280*(6), 518–545.

Logan, J. M., J. R. Drobe, and W. C. McClelland (2000), Geology of the Forrest Kerr-Mess Creek Area, Northwestern British Columbia (104B/10, 15, & 104G/2 & 7W), Ministry of Employment and Investment, *Geoscience Map*, *3*(1), 100–000.

Lund, K., J. N. Aleinikoff, E. Y. Yacob, D. M. Unruh, and C. M. Fanning (2008), Coolwater culmination: Sensitive high-resolution ion microprobe (SHRIMP) U-Pb and isotopic evidence for continental delamination in the Syringa Embayment, Salmon River suture, Idaho, *Tectonics*, *27*, TC2009, doi:10.1029/2006TC002071.

Marsden, H., and D. J. Thorkelson (1992), Geology of the Hazelton volcanic belt in British Columbia: Implications for the Early to Middle Jurassic evolution of Stikinia, *Tectonics*, *11*, 1266–1287, doi:10.1029/92TC00276.

Matzel, J. E. P., S. A. Bowring, and R. B. Miller (2004), Protolith age of the Swakane Gneiss, North Cascades, Washington: Evidence of rapid underthrusting of sediments beneath an arc, *Tectonics*, *23*, TC6009, doi:10.1029/2003TC001577.

McClelland, W. C., G. E. Gehrels, S. D. Samson, and P. J. Patchett (1992a), Protolith relations of the Gravina Belt and Yukon-Tanana terrane in central southeastern Alaska, *J. Geol.*, *100*(1), 107–123.

McClelland, W. C., G. E. Gehrels, S. D. Samson, and P. J. Patchett (1992b), Structural and geochronological relations along the western flank of the Coast Mountains batholith-Stikine River to Cape Fanshaw, central southeastern Alaska, *J. Struct. Geol.*, *14*(4), 475–489.

McClelland, W. C., G. E. Gehrels, and J. B. Saleeby (1992c), Upper Jurassic-Lower Cretaceous basinal strata along the Cordilleran margin—Implications for the accretionary history of the Alexander-Wrangellia-Peninsular terrane, *Tectonics*, *11*, 823–835.

Mezger, K., and E. J. Krogstad (1997), Interpretation of discordant U-Pb zircon ages: An evaluation, *J. Metamorph. Geol.*, *15*(1), 127–140, doi:10.1111/j.1525-1314.1997.00008.x.

Monger, J. (1977), Upper Paleozoic rocks of the northwestern British Columbia, Geological Survey of Canada, Paper, 77-1A, 255–262.

Monger, J. W. H., R. A. Price, and D. J. Tempelman-Kluit (1982), Tectonic accretion and the origin of the two major metamorphic and plutonic welts in the Canadian Cordillera, *Geology*, *10*, 70–75.

Monger, J., J. O. Wheeler, H. W. Tipper, H. Gabrielse, T. Harms, L. C. Struik, R. B. Campbell, C. J. Dodds, G. E. Gehrels, and J. O'Brien (1991), Part B. Cordilleran terranes, in edited by H. Gabrielse and C. J. Yorath, *Upper Devonian to Middle Jurassic assemblages*, chapter 8 of Geology of the Cordilleran Orogen in Canada, *Geol. Surv.Can. Geol. Can.*, 4, 281–327.

Monger, J. W. H., P. van der Heyden, J. M. Journeay, C. A. Evenchick, and J. B. Mahoney (1994), Jurassic-Cretaceous basins along the Canadian Coast Belt: Their bearing on pre-mid-Cretaceous sinistral displacements, *Geology*, *22*(2), 175–178.

Nelson, J. L. (2009), Terrace Regional Mapping Project, year 4: Extension of Paleozoic volcanic belt and indicators of volcanogenic massive sulphide-style mineralization near Kitimat, British Columbia (NTS 103I/02, 07), *Geol. Fieldwork*, *2008*, 7–20.

Otamendi, J. E., M. N. Ducea, A. M. Tibaldi, G. W. Bergantz, J. D. de la Rosa, and G. I. Vujovich (2009), Generation of tonalitic and dioritic magmas by coupled partial melting of gabbroic and metasedimentary rocks within the deep crust of the Famatinian magmatic arc, Argentina, *J. Petrol.*, *50*(5), 841–873, doi:10.1093/Petrology/Egp022.

Patchett, P. J., and G. E. Gehrels (1998), Continental influence on Canadian Cordilleran terranes from Nd isotopic study, and significance for crustal growth processes, *J. Geol.*, *106*(3), 269–280, doi:10.1086/516021.

Patchett, P. J., G. E. Gehrels, and C. E. Isachsen (1998), Nd isotopic characteristics of metamorphic and plutonic rocks of the Coast Mountains near Prince Rupert, British Columbia, *Can. J. Earth Sci.*, *35*(5), 556–561.

Patiño Douce, A. E., E. D. Humphreys, and A. D. Johnston (1990), Anatexis and metamorphism in tectonically thickened continental crust exemplified by the Sevier hinterland, western North America, *Earth Planet. Sc. Lett.*, *97*(3–4), 290–315.

Pavlis, T. L., and S. M. Roeske (2007), The Border Ranges fault system, southern Alaska, in Special Paper 431: Tectonic Growth of a Collisional Continental Margin: Crustal Evolution of Southern Alaska, *Geol. Soc. Am. Bull.*, *431*, 95–127.

Pavlis, T. L., and V. B. Sisson (1995), Structural history of the Chugach metamorphic complex in the Tana River region, eastern Alaska: A record of Eocene ridge subduction, *Geol. Soc. Am. Bull. Bulletin*, *107*(11), 1333–1355.

Pecha, M. E., G. E. Gehrels, W. C. McClelland, D. Giesler, C. White, and I. Yokelson (2016), Detrital zircon U-Pb geochronology and Hf isotope geochemistry of the Yukon-Tanana terrane, Coast Mountains, southeast Alaska, *Geosphere*, *12*(5), 1556–1574, doi:10.1130/GES01303.1.

Philpotts, A. R. (1990), *Principles of Igneous and Metamorphic Petrology*, Prentice Hall, Englewood Cliffs, N. J.

Pidgeon, R. T. (1992), Recrystallisation of oscillatory zoned zircon: Some geochronological and petrological implications, *Contrib. Mineral. Petrol.*, *110*(4), 463–472, doi:10.1007/BF00344081.

Pignotta, G. S., J. L. Meyers, J. B. Mahoney, and B. G. Hardel (2010), Geochemical characterization and geochronology of the Paleozoic Mt. Attree Volcanic Complex, Terrace, British Columbia, NTS 103I, Association for Mineral Exploration BCs Mineral Exploration Roundup.

Plafker, G., W. J. Nokleberg, and J. S. Lull (1989), Bedrock geology and tectonic evolution of the Wrangellia, Peninsular, and Chugach terranes along the trans-Alaska crustal transect in the Chugach Mountains and southern Copper River Basin, Alaska, *J. Geophys. Res.*, *94*, 4255–4295, doi:10.1029/JB094iB04p04255.

Roddick, J. A. (1970), Douglas Channel-Hecate Strait map-area, *Geol. Surv. Can. Pap.*, *70-41*, 56.

Roddick, J. A., and W. W. Hutchison (1972), Plutonic and associated rocks of the Coast Mountains of British Columbia: Guidebook for excursion AC04, vol. 24, 24th International Geological Congress.

Roeske, S. M., L. W. Snee, and T. L. Pavlis (2003), Dextral-slip reactivation of an arc-forearc boundary during Late Cretaceous-early Eocene oblique convergence in the northern Cordillera, in *Geology of a Transpressional Orogen Developed During Ridge-Trench Interaction Along the North Pacific Margin*, edited by V. B. Sisson, S. M. Roeske and T. L. Pavlis, *Geol. Soc. Am. Bull. Memoir*, 371, 141–169.

Rubatto, D. (2002), Zircon trace element geochemistry: Partitioning with garnet and the link between U-Pb ages and metamorphism, *Chem. Geol.*, *184*(1–2), 123–138.

Rubin, C. M., and J. B. Saleeby (1992), Tectonic history of the eastern edge of the Alexander Terrane, southeast Alaska, *Tectonics*, *11*(3), 586–602, doi:10.1029/91TC02182.

Rubin, C. M., J. B. Saleeby, D. S. Cowan, M. T. Brandon, and M. F. Mcgroder (1990), Regionally extensive midcretaceous west-vergent thrust system in the northwestern Cordillera—Implications for continent-margin tectonism, *Geology*, *18*(3), 276–280.

Rusmore, M. E., G. Gehrels, and G. J. Woodsworth (2001), Southern continuation of the coast shear zone and Paleocene strain partitioning in British Columbia-southeast Alaska, *Geol. Soc. Am. Bull. Bulletin*, *113*(8), 961–975.

Rusmore, M. E., G. J. Woodsworth, and G. E. Gehrels (2005), Two-stage exhumation of midcrustal arc rocks, Coast Mountains, British Columbia, *Tectonics*, *24*, TC5013, doi:10.1029/2004TC001750.

Saleeby, J. (2003), Segmentation of the Laramide slab—Evidence from the southern Sierra Nevada region, *Geol. Soc. Am. Bull. Bulletin*, *115*(6), 655–668.

Samson, S. D., and P. J. Patchett (1991), The Canadian Cordillera as a modern analogue of Proterozoic crustal growth, *Australian Journal of Earth Sciences*, *38*(5), 595–611, doi:10.1080/08120099108727994.

Samson, S. D., P. J. Patchett, W. C. McClelland, and G. E. Gehrels (1991), Nd isotopic characterization of metamorphic rocks in the Coast Mountains, Alaskan and Canadian Cordillera: Ancient crust bounded by juvenile terranes, *Tectonics*, *10*, 770–780, doi:10.1029/90TC02732.

Schaltegger, U., C. Fanning, D. Gunther, J. Maurin, K. Schulmann, and D. Gebauer (1999), Growth, annealing and recrystallization of zircon and preservation of monazite in high-grade metamorphism: Conventional and in-situ U-Pb isotope, cathodoluminescence and microchemical evidence, *Contrib. Mineral. Petrol.*, *134*, 186–201.

Scharman, M. R., and T. L. Pavlis (2012), Kinematics of the Chugach metamorphic complex, southern Alaska: Plate geometry in the north Pacific margin during the Late Cretaceous to Eocene, *Tectonics*, *31*, TC4014, doi:10.1029/2011TC003034.

Selverstone, J., and L. S. Hollister (1980), Cordierite-bearing granulites from the Coast Ranges, British Columbia; P-T conditions of metamorphism, *Can. Mineral.*, *18*, 119–129.

Sisson, V. B., and T. L. Pavlis (1993), Geologic consequences of plate reorganization: An example from the Eocene southern Alaska fore arc, *Geology*, *21*(10), 913.

Spencer, K. J., B. R. Hacker, A. R. C. Kylander-Clark, T. B. Andersen, J. M. Cottle, M. A. Stearns, J. E. Poletti, and G. G. E. Seward (2013), Campaign-style titanite U-Pb dating by laser-ablation ICP: Implications for crustal flow, phase transformations and titanite closure, *Chem. Geol.*, *341*(C), 84–101, doi:10.1016/j.chemgeo.2012.11.012.

Stacey, J. S., and J. D. Kramers (1975), Approximation of terrestrial lead isotope evolution by a 2-stage model, *Earth Planet. Sci. Lett.*, *26*, 207–221.

Stowell, H. H., and M. L. Crawford (2000), Metamorphic history of the Coast Mountains orogen, western British Columbia and southeastern Alaska, in *Tectonics of the Coast Mountains, southeastern Alaska and British Columbia*, edited by H. H. Stowell and W. C. McClelland, *Geol. Soc. Am. Bull. Spec. Pap., 343*, 257–283.

Tipper, H. W., and T. A. Richards (1976), Jurassic stratigraphy and history of north-central British Columbia, Geological Survey of Canada.

Tochilin, C. J., G. E. Gehrels, J. Nelson, and J. B. Mahoney (2014), U-Pb and Hf isotope analysis of detrital zircons from the Banks Island assemblage (coastal British Columbia) and southern Alexander terrane (southeast Alaska), *Lithosphere*, *6*(3), 200–215, doi:10.1130/L338.1.

Wasserburg, G. J., S. B. Jacobsen, D. J. DePaolo, M. T. McCulloch, and T. Wen (1981), Precise determination of Sm/Nd ratios, Sm and Nd isotopic abundances in standard solutions, *Geochim. Cosmochim. Acta*, *45*, 2311–2323.

Wetmore, P. H., and M. N. Ducea (2011), Geochemical evidence of a near-surface history for source rocks of the central Coast Mountains batholith, British Columbia, *Int. Geol. Rev.*, *53*(2), 230–260, doi:10.1080/00206810903028219.

Wheeler, J. O., and P. McFeely (1991), Tectonic assemblage map of the Canadian Cordillera, Geological Survey of Canada Map, 1712A, scale 1:2,000,000.

White, C., G. E. Gehrels, M. Pecha, D. Giesler, I. Yokelson, W. C. McClelland, and R. F. Butler (2015), U-Pb and Hf isotope analysis of detrital zircons from Paleozoic strata of the southern Alexander terrane (southeast Alaska), *Lithosphere*, *8*(1), 83–96, doi:10.1130/L475.1.

Wolf, D. E., C. L. Andronicos, and J. D. Vervoort (2010), Thermal evolution of the Central Gneiss Complex, British Columbia, constrained by garnet geochronology, *GeoCanada*, *2010*, 4.

Woodsworth, G. J. (1979), Geology of Whitesail Lake map area, British Columbia, *Geol. Surv. Canada Curr. Res.*, *79-IA*, 25–29.

Woodsworth, G. J., M. L. Crawford, and L. S. Hollister (1983a), Metamorphism and structure of the Coast Plutonic Complex and adjacent belts, Prince Rupert and Terrace areas, British Columbia, *Geol. Assoc. Can. Field Trip Guidebook*, *14*, 62.

Woodsworth, G. J., W. D. Loveridge, R. R. Parrish, and R. W. Sullivan (1983b), Uranium-lead dates from the Central Gneiss Complex and Ecstall pluton, Prince Rupert map area, British Columbia, *Can. J. Earth Sci.*, *20*(9), 1475–1483.

Yonkee, W. A., and A. B. Weil (2015), Tectonic evolution of the Sevier and Laramide belts within the North American Cordillera orogenic system, *Earth-Sci. Rev.*, *150*(C), 1–63, doi:10.1016/j.earscirev.2015.08.001.

Yokelson, I., G. E. Gehrels, M. Pecha, D. Giesler, C. White, and W. C. McClelland (2015), U-Pb and Hf isotope analysis of detrital zircons from Mesozoic strata of the Gravina belt, southeast Alaska, *Tectonics*, *34*, 2052–2066, doi:10.1002/2015TC003955.